PHILOSOPHICAL TRANSACTIONS B

royalsocietypublishing.org/journal/rstb

Review

Cite this article: Salvage SC, Dulhunty AF, Jeevaratnam K, Jackson AP, Huang CL-H. 2023 Feedback contributions to excitation–contraction coupling in native functioning striated muscle. *Phil. Trans. R. Soc. B* **378**: 20220162.
https://doi.org/10.1098/rstb.2022.0162

Received: 8 July 2022
Accepted: 13 October 2022

One contribution of 23 to a theme issue 'The heartbeat: its molecular basis and physiological mechanisms'.

Subject Areas:
physiology, cellular biology, biophysics

Keywords:
T-SR junction, ryanodine receptor, Na^+ channel, C-terminal domains, III-IV linker, Ca^{2+} regulation

Author for correspondence:
Christopher L.-H. Huang
e-mail: clh11@cam.ac.uk

THE ROYAL SOCIETY PUBLISHING

Feedback contributions to excitation–contraction coupling in native functioning striated muscle

Samantha C. Salvage[1], Angela F. Dulhunty[2], Kamalan Jeevaratnam[3], Antony P. Jackson[1] and Christopher L.-H. Huang[1,3,4]

[1]Department of Biochemistry, University of Cambridge, Tennis Court Road, Cambridge CB2 1QW, UK
[2]Eccles Institute of Neuroscience, John Curtin School of Medical Research, The Australian National University, 131 Garran Road, Acton 2601, Australia
[3]Faculty of Health and Medical Sciences, University of Surrey, Daphne Jackson Road, Guildford GU2 7XH, UK
[4]Physiological Laboratory, University of Cambridge, Downing Street, Cambridge CB2 3EG, UK

SCS, 0000-0002-5793-2349; AFD, 0000-0001-9493-4944; CL-HH, 0000-0001-9553-6112

Skeletal and cardiac muscle excitation–contraction coupling commences with $Na_v1.4/Na_v1.5$-mediated, surface and transverse (T-) tubular, action potential generation. This initiates *feedforward*, allosteric or Ca^{2+}-mediated, T-sarcoplasmic reticular (SR) junctional, voltage sensor-Cav1.1/Cav1.2 and ryanodine receptor-RyR1/RyR2 interaction. We review recent structural, physiological and translational studies on possible *feedback* actions of the resulting SR Ca^{2+} release on $Na_v1.4/Na_v1.5$ function in native muscle. Finite-element modelling predicted potentially regulatory T-SR junctional $[Ca^{2+}]_{TSR}$ domains. $Na_v1.4/Na_v1.5$, III-IV linker and C-terminal domain structures included Ca^{2+} and/or calmodulin-binding sites whose mutations corresponded to specific clinical conditions. Loose-patch-clamped native murine skeletal muscle fibres and cardiomyocytes showed reduced Na^+ currents (I_{Na}) following SR Ca^{2+} release induced by the Epac and direct RyR1/RyR2 activators, 8-(4-chlorophenylthio)adenosine-3′,5′-cyclic monophosphate and caffeine, abrogated by the RyR inhibitor dantrolene. Conversely, dantrolene and the Ca^{2+}-ATPase inhibitor cyclopiazonic acid increased I_{Na}. Experimental, catecholaminergic polymorphic ventricular tachycardic *RyR2-P2328S* and metabolically deficient $Pgc1\beta^{-/-}$ cardiomyocytes also showed reduced I_{Na} accompanying $[Ca^{2+}]_i$ abnormalities rescued by dantrolene- and flecainide-mediated RyR block. Finally, hydroxychloroquine challenge implicated action potential (AP) prolongation in slowing AP conduction through modifying Ca^{2+} transients. The corresponding tissue/organ preparations each showed pro-arrhythmic, slowed AP upstrokes and conduction velocities. We finally extend discussion of possible Ca^{2+}-mediated effects to further, Ca^{2+}, K^+ and Cl^-, channel types.

This article is part of the theme issue 'The heartbeat: its molecular basis and physiological mechanisms'.

1. Feedforward versus feedback events in striated muscle excitation–contraction coupling

Skeletal and cardiac muscle excitation–contraction coupling commences with Na^+ channel, $Na_v1.4$ or $Na_v1.5$, mediated action potential (AP) initiation and propagation through their surface and transverse (T-) tubular membranes. Tubular Cav1.1 or Cav1.2 channels then sense the resulting voltage changes and transduce these into a ryanodine receptor (RyR1 or RyR2)-mediated sarcoplasmic reticular (SR) Ca^{2+} store release. This takes place through either reciprocal allosteric Cav1.1-RyR1 [1] or Ca^{2+}-induced Cav1.2-RyR2 coupling in skeletal or cardiac muscle, respectively [2]. Release of intracellularly stored

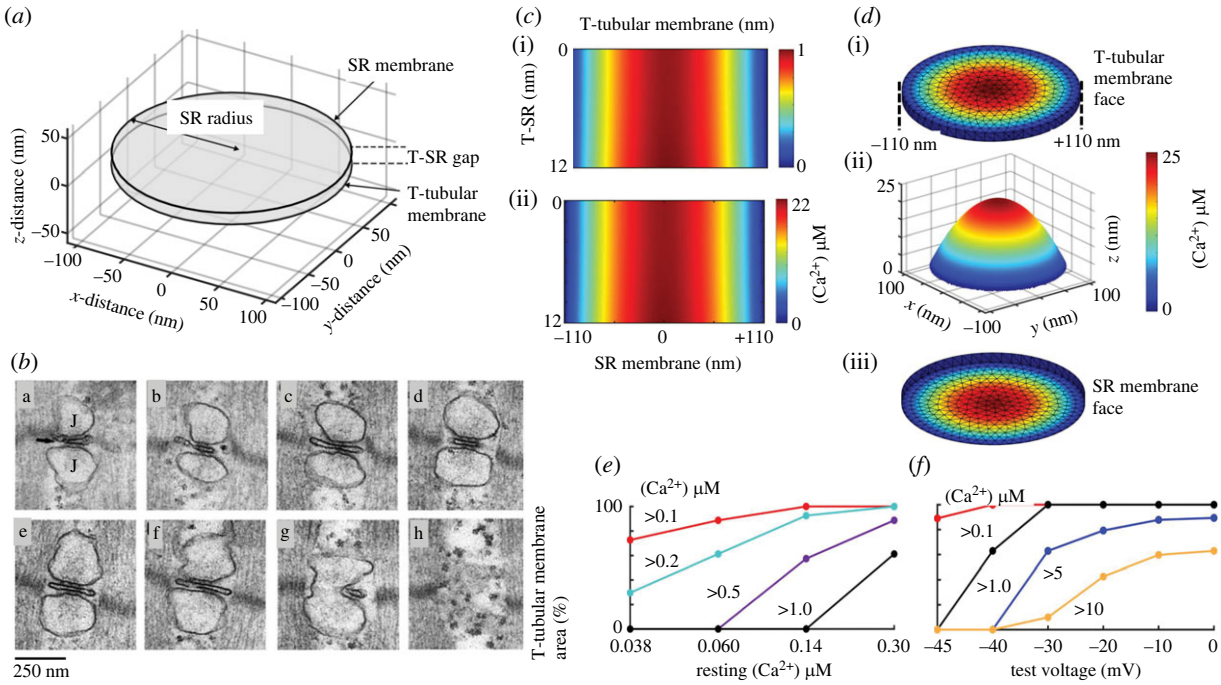

Figure 1. Model Ca^{2+} microdomain formation in the T-SR junction. (*a*) Formalized tubular (T) and SR membrane discs, radial (*xy*) diameter, $d = 220$ nm, separated by axial (*z*) T-SR distance, $w = 12$ nm, representing (*b*) amphibian muscle T-SR junction geometry, shown in serial electron microscope sections (a–h). (*c*,*d*) $[Ca^{2+}]$ modelling results in (*c*) midline axial views in (i) resting and (ii) activated amphibian skeletal muscle, and (*d*) (i) radial and (ii) perspective T-tubular and (iii) radial SR membrane mapping of $[Ca^{2+}]$ following activation. (*e*,*f*) Proportions of tubular membrane exposed to different $[Ca^{2+}]_i$ (*e*) in resting muscle assuming different resting bulk cytosolic $[Ca^{2+}]_i$ and (*f*) following activation to different membrane potentials V_m (from figure 2 of Martin *et al.* [6] and figures 1 and 2A,B,D,F, 7C and 8a,B of Bardsley *et al.* [7] by permission).

SR Ca^{2+} then results in the elevation of bulk cytosolic Ca^{2+} concentration, $[Ca^{2+}]_i$, that activates troponin, in turn triggering the myofilament action that causes myocyte contraction. However, in addition to these *feedforward* processes, recent speculations have considered possible *feedback* modulation of this process for which one example might involve a long loop Ca^{2+}-mediated feedback signalling influencing the Na^+ channel itself. This action would be consistent with the function of intracellular Ca^{2+} in acting as a strategic second messenger known to regulate widespread protein activity through numerous cell types.

We here review recent evidence for such a mechanism as applied to intact native functioning skeletal and cardiac muscle. We explore the possible anatomical and molecular background suggested by theoretical and experimental structural studies for such schemes, then examine evidence for its possible electrophysiological operation in native intact skeletal and cardiac muscle. These insights are translated into experimental and clinical human disease models. This involves first summarizing cell modelling and molecular background evidence bearing on the necessary diffusional and structural conditions of elevated Ca^{2+} and $Na_v1.4/Na_v1.5$ structures required for Ca^{2+} feedback action. These features are next related to results of loose-patch clamp studies exploring for alterations in voltage-dependent Na^+ current densities, I_{Na}, half-maximal activation and inactivation voltages $V_{1/2}$, and steepness factors, *k*, following manipulations of intracellular $[Ca^{2+}]$ in native skeletal muscle fibres and cardiomyocytes. The latter employed the Exchange protein directly activated by cAMP (Epac) and RyR1/RyR2 activators, 8-(4-chlorophenylthio)adenosine-3′,5′-cyclic monophosphate (8-CPT) and caffeine, using as controls the RyR1/RyR2 inhibitor dantrolene, and the RyR1/RyR2 and Ca^{2+}-ATPase inhibitors dantrolene and cyclopiazonic acid (CPA). Genetic disease and other chronic clinical models similarly permitted correlations between reduced I_{Na} and $[Ca^{2+}]_i$ changes and their specific pharmacological rescue. These included studies on murine gain of function, *RyR2-P2328S*, catecholaminergic polymorphic ventricular tachycardic (CPVT) and loss-of-function $Pgc1\beta^{-/-}$ paradigms for pro-arrhythmic metabolic cardiac disease. Findings were related to physiological effects bearing on the consequent velocity of propagation of cell excitability and its translational consequences in intact organs. We finally discuss reports describing hydroxychloroquine (HCQ) challenge and the possibility of a Ca^{2+} modulation arising from altered Ca^{2+} release transients consequent upon prolonged AP recovery. We conclude speculating on possible roles for Ca^{2+}-mediated feedback regulation as a general phenomenon that might similarly affect other, Ca^{2+}, K^+ and Cl^-, channel activity *in vivo*.

2. Potential regulatory Ca^{2+} microdomains in the transverse tubule-sarcoplasmic reticular junction

Structural descriptions of skeletal or cardiac muscle, sarcomeres and their surface, T-tubular and SR membranes localize the processes coupling T-tubular membrane potential changes and SR Ca^{2+} release to T-SR triadic or dyadic junctions [3–5]. These constitute regions where $Na_v1.4/Na_v1.5$-expressing T-tubular membranes come into close geometrical relationship with, while remaining electrically isolated from, the RyR1/RyR2-expressing terminal cisternal SR membranes. They thus form regions where both feedforward and Ca^{2+}-mediated feedback actions could take place. Their quantitative detailed anatomy appears compatible with the latter function. It can

be quantified (figure 1*a*) using findings from serially sectioned electron microscope images, here exemplified for amphibian skeletal muscle fibres (figure 1*b*) [6]. T-SR junctional regions taking the form of triad or dyad junctions in skeletal or cardiac muscle, respectively, form restricted diffusion spaces bounded by their component T-tubular or SR membranes in parallel, approximately 100–400 nm, alignment. These would potentially permit ion accumulation or depletion. Here, local Ca^{2+} release might elevate their $[Ca^{2+}]_{TSR}$ to levels sufficient to mediate regulatory feedback effects.

Fluorescent Ca^{2+} indicator results were compatible with such $[Ca^{2+}]_{TSR}$ microdomains with their small dimensions and dispersed nature [8–10]. These compared experimental kinetic and steady state signals from introduced Ca^{2+} sensors localized to T-SR gap regions. This involved Ca^{2+} sensor conjugation to FKBP12.6 [8], triadin [10] or the $Ca_v1.1$ $\gamma1$ auxiliary subunit [10]. This permitted comparisons of their $[Ca^{2+}]$ with those existing in the bulk cardiac [8] or skeletal muscle cytosol [10], albeit admitting unproven assumptions of equal cleft and bulk concentrations of the Ca^{2+} probes [10]. The findings suggested differing resting T-SR regional (194 nM) and bulk cytosolic $[Ca^{2+}]$ (100 nM) attributable to background SR Ca^{2+} leak [8]. Following activation of excitation–contraction coupling, fluorescence from untargeted Ca^{2+} probes was distributed throughout the muscle fibres with large Ca^{2+}-dependent changes and obvious kinetic delays [10]. T-SR junctional $[Ca^{2+}]$ more rapidly reached distinct maximum values distinctly higher [8] or lower [10] compared to corresponding findings in bulk $[Ca^{2+}]$. These findings prompted preliminary modelling explorations of the functions of possible dedicated and promiscuous calmodulin pools, respectively, directly regulating channel activity and sensing local Ca^{2+} to trigger downstream Ca^{2+}/CaM-dependent protein kinase II and calcineurin [9].

Subsequent quantitative, finite-element diffusional modelling of RyR1/RyR2-mediated Ca^{2+} release and its subsequent fluxes and consequent concentrations through the T-SR junction used as geometrical parameters their established distributions, densities and ultrastructure in amphibian skeletal muscle [7]. Such modelling employed previously experimentally quantified SR Ca^{2+} release rates in response to varying test voltage steps [11]. It predicted that T-SR junctional regions could both accumulate and deplete released SR Ca^{2+} in both activated and resting muscle fibres [7]. The predicted RyR-mediated Ca^{2+} influx densities J_{influx} across the SR membrane face of each T-SR junction gave rise to a Ca^{2+} diffusion through a radially symmetric T-SR junctional space (figure 1*c*,*d*). This was followed by its first-order diffusional efflux at the edge of the modelled junction into the well-stirred cytosolic space. Here the modelling correctly replicated previously observed bulk cytosolic $[Ca^{2+}]_i$, before similarly replicating their eventual first-order SERCA-mediated Ca^{2+} SR re-sequestration [12].

The resulting Ca^{2+} microdomains showed local $[Ca^{2+}]_{TSR}$ ranging from approximately 0.3–0.4 to 17–20 µM at voltages corresponding to contraction threshold and full activation, respectively. These traversed the entire axial T-SR distance (figure 1*c*) with radial, greater than fivefold, $[Ca^{2+}]$ differences between T-SR junction centre and edge (figure 1*d*i–iii). The Ca^{2+} microdomains robustly persisted through 10^4-fold variations in Ca^{2+} diffusion coefficient, and fivefold variations in T-SR distance and diameter, at constant J_{influx}, and 10- and 100-fold J_{influx} reductions below threshold levels of Ca^{2+} release. Finally, they also persisted giving T-SR centre $[Ca^{2+}]$ at µM levels at J_{influx} corresponding to reported bulk cytosolic $[Ca^{2+}]_i$ even in resting as opposed to activated muscle [13–15]. Significant proportions of resting T-tubular membrane then experienced significant, approximately 0.5 µM, $[Ca^{2+}]$ through typical reported resting bulk cytosolic $[Ca^{2+}]$ values (figure 1*e*). In such simulations, muscle activation by successively larger depolarizing steps recruited correspondingly greater proportions of T-tubular membrane that experienced successively higher, 0.1 to 10 µM, $[Ca^{2+}]$ (figure 1*f*).

The resulting local $[Ca^{2+}]_{TSR}$ microdomains generated by RyR-mediated Ca^{2+} release could then access T-tubular $Na_v1.4$ or $Na_v1.5$ channels in the T-SR junction vicinity. The available evidence could prompt similar future studies extending to cardiac $Na_v1.5$ as opposed to skeletal muscle $Na_v1.4$ channels. Mammalian atrial and ventricular cardiomyocyte junctions between surface and SR membranes differ from those in skeletal muscle in involving peripheral couplings or dyadic rather than triadic junctions [4]. Nevertheless the detailed organization and separation of their participating T-tubular and SR membranes remain similar and therefore are similarly compatible with junctional Ca^{2+} domain formation [16].

3. Ca^{2+} and Ca^{2+}-calmodulin regulatory domains in voltage-sensitive Na^+ channels

Recent cryo-electron microscope characterizations of $Na_v1.4$/$Na_v1.5$ structure are consistent with an existence of molecular regions that might be involved in a Ca^{2+}-mediated feedback modulation. These are distinct from regions previously implicated in rapid channel activation events. However, they are compatible with interactions with those $Na_v1.4$/$Na_v1.5$ regions involved in the subsequent, slower, channel inactivation events. Excitation–contraction coupling *feedforward* mechanisms thus commence with $Na_v1.4$ or $Na_v1.5$ activation by voltage-sensitive outward transitions of positively charged residues in voltage-sensing S4 helices in the outer rim of their domains DI-III (figure 2*a*i; [18–21]). Coupled conformational changes in the channel pore, S5 and S6 helices, then drive the resting, *closed* to *open*, activated transition, permitting the inward, depolarizing, transmembrane Na^+ fluxes initiating cell excitation. However, activation is then followed by channel pore closure into an *inactivated* state [18,22]. This is the consequence of slower outward DIV S4 helix movements. These allow binding of a hydrophobic IFM (isoleucine, phenylalanine and methionine) motif within the cytoplasmic III-IV linker to a hydrophobic pocket between domains III and IV (figure 2*a*ii). The latter entities could be involved in additional *feedback* Ca^{2+} regulatory events through further interactions with a globular, intracellular C-terminal domain (CTD) flexibly connected to the Na_v DIV S6 helix.

CTDs begin at residues 1599 on $Na_v1.4$ and 1773 on $Na_v1.5$ with a sequence of five α-helical regions fitting the EF-like hand (EFL) consensus sequence [23], a sixth α-helical region and further more disordered and less-well structurally characterized regions. The EFL contains a prominent cleft bounded by helices 1 and 5, with helix 4 forming its floor [24]. In resting $Na_v1.x$, this can form complexing salt bridges with site A (residues 1490–1503) of the DIII-IV linker constraining the IFM motif [25,26]. With channel opening and outward movement of the DIV S4 helix, the salt bridges are disrupted. This dissociates CTD from the DIII-DIV

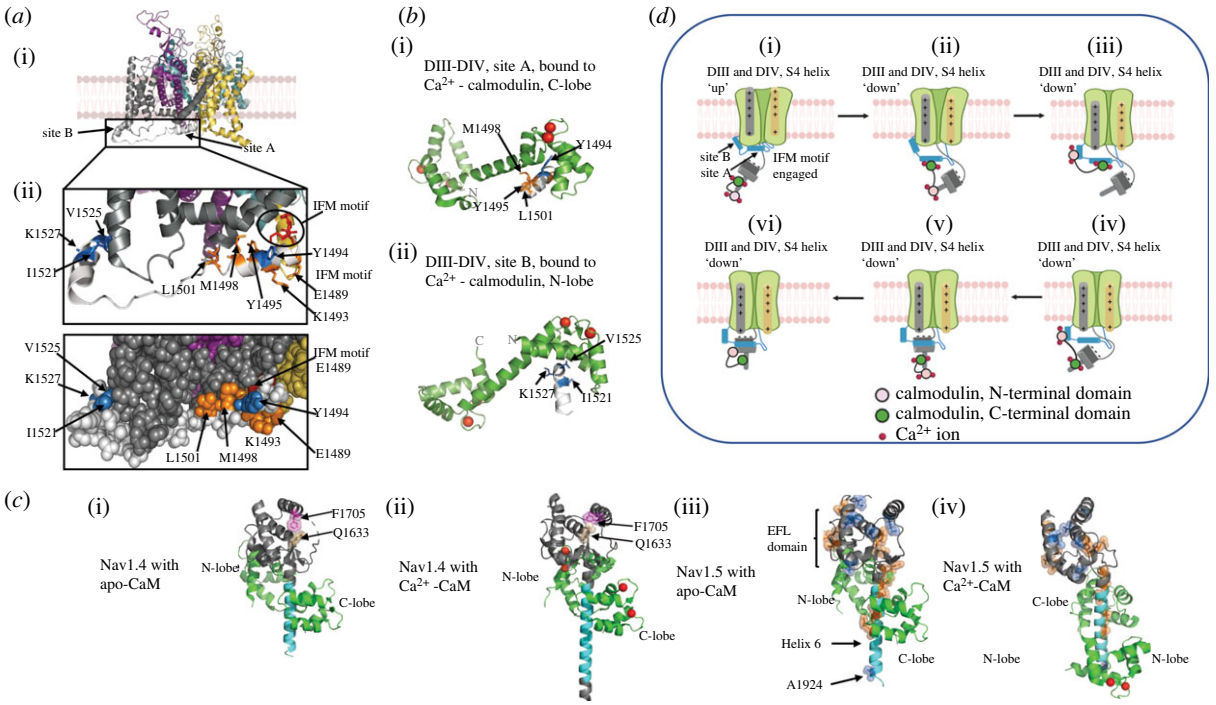

Figure 2. Regulatory-binding sites on the voltage-gated Na^+ channels. (*a*) $Na_v1.5$ channel showing DIII-DIV linker region in grey (i) and at closer resolution (ii) with binding sites A and B marked. (*b*) Ca^{2+}-calmodulin (CaM) C-lobe (i) and N-lobe binding (ii), respectively, to site A and site B helices. Residues associated with clinical phenotypes marked and coloured. (*c*) Apo-CaM (i,iii) or Ca^{2+}-CaM (ii, iv) binding to $Na_v1.4$ (i, ii) and $Na_v1.5$ (iii, iv) CTDs in side view. Ca^{2+} shown as red balls. Myotonia and PMC-associated residues highlighted in tan and purple in the $Na_v1.4$ structures (i,ii). LQTS and BrS-associated residues highlighted in orange and sky blue, respectively, in the $Na_v1.5$ structures (iii,iv). (*c*) CaM-binding patterns and possible actions on $Na_v1.5$ recovery from inactivation. (*d*) (i) IFM motif and DIII-DIV linker fully engaged with α subunit; CTD dissociated from site A in the inactivated state with Ca^{2+}-CaM bound to helix 6 (PDB structure 4jq0). (*d*) (ii)–(v) Conformational interactions arranged in a possible sequential channel recovery from inactivation. (vi) Proposed $Na_v1.5$ conformation after return to resting state. If Ca^{2+} levels are low, the predominant apo-CaM binds to helix 6 (PDB structure 4ovn) (By permission from figures 2b,C, 3B, 4B of Salvage *et al.* [17]).

linker, freeing the IFM motif to transition into the inactivated state. The latter allows restoration of the resting membrane potential (figure 2*a*ii).

Ca^{2+}-binding acidic residues of $Na_v1.5$ CTD EFLs [23,27,28] lie along the outward face of helix 1 rather than within the turn loops between adjacent α-helices elsewhere associated with high Ca^{2+} affinity [24,29,30]. Nevertheless, both DIII-IV linker and CTD show potential regulatory sites that can bind the established nM-low μM K_d Ca^{2+} sensor calmodulin, CaM [31–33]. CaM includes N- and C-lobes each possessing two Ca^{2+}-binding EF hands (figure 2*b*i,ii). Ca^{2+}-free, apo- and Ca^{2+} bound, and Ca^{2+}-CaM, respectively, show 'closed' and 'semi-open' and 'open' and 'semi-open' states. The 'open' and 'semi-open' states show EF hand helix orientations exposing a hydrophobic groove able to bind particular α-helical protein sequence motifs.

The various binding properties of these N- and C- lobes of apo- and Ca^{2+}-CaM respectively to the DIII-DIV linker and CTD give rise to a range of possible interactions between CaM and the $Na_v1.4$/$Na_v1.5$. First, Ca^{2+}-CaM but not apo-CaM, via its N- and C-lobes, binds to isolated, purified *DIII-DIV linker domains* at sites B (1500–1530) and A (1490–1503), respectively (figure 2*b*i,ii) [34,35]. The latter is additional to site A's ability to bind the CTD EFL cleft. $Na_v1.5$ DIII-DIV linker and CTD co-precipitation is thus catalysed by Ca^{2+}-CaM, but inhibited by the Ca^{2+}-chelator, EGTA [36]. Second, CTDs bind the *CaM* with potential regulatory effects [37,38]. The IQ motif within helix 6 of the $Na_v1.4$ or $Na_v1.5$ [39] CTD EFL [40] can bind the 'semi-open state' apo-CaM C-lobe [31]. Additionally, both helix 3 and the N-terminal of helix 6 can bind the 'closed-state' apo-CaM N-lobe (figure 2*c*i,iii). The IQ motif (figure 2*c*ii,iv) can also bind the 'semi-open state' Ca^{2+}-CaM C-lobe. In $Na_v1.5$, a downstream slightly overlapping N-lobe-binding motif (NLBM) can then bind a shifted Ca^{2+}-CaM N-lobe (figure 2*c*iv). $Na_v1.4$ contrastingly lacks a functioning NLBM [41] leaving the Ca^{2+}-CaM N-lobe free to interact elsewhere, potentially the III-IV linker B-site (figure 2*c*ii) [35,42,43]. In either event, simultaneous binding of either site A or B of the DIII-DIV linker, to their respective Ca^{2+}-CaM C or N-lobes, and the remaining α-subunit in an inactivated $Na_v1.4$ or $Na_v1.5$ thus becomes unlikely.

These binding properties result in a variety of potential interaction patterns between apo- and Ca^{2+} calmodulin, and the DIII-DIV linker and CTD of $Na_v1.4$/$Na_v1.5$. The Ca^{2+}-CaM then could bind to the CTD in an inactivated $Na_v1.5$ (figure 2*d*i). Freeing sites A and B to permit such binding would require IFM motif disengagement from its binding site (figure 2*d*ii). The binding could involve the pair of Ca^{2+}-CaM N and/or C lobes, respectively, capable of binding exclusively to either the III-IV linker (figure 2*d*iii; [35]) or the CTD (figure 2*d*i, v,vi; [30]). Alternatively the Ca^{2+}-CaM could cross-link between them whether involving the $Na_v1.5$ NLBM (figure 2*d*ii; [34]) or $Na_v1.4$ IQ domain (figure 2*d*iv; [44]).

These patterns could form a speculative recovery sequence from inactivation to the channel resting state involving modulation through direct or CaM-mediated Ca^{2+} binding (figure 2*d*i–vi) [17]. A binding of one or both Ca^{2+}-CaM lobes to the DIII-DIV linker (figure 2*d*iii; [35]) might then potentiate recovery from inactivation. Conversely, Ca^{2+} binding to the CaM C-lobe reduces its affinity for the CTD [34,42] enhancing $Na_v1.5$ inactivation (figure 2*d*ii) [34]. Finally, Ca^{2+}-CaM

binding to the III-IV linker could also modify recovery from inactivation by precluding (figure 2*d*ii–iv) direct CTD association with the III-IV linker (figure 2*d*v,vi).

An existence of further potentially regulatory $Na_v1.5$ channel sites may be reflected in increases in late Na^+ current (I_{NaL}) causing delayed AP repolarization as occurs in long QT type 3 syndrome (LQTS3). Effects of KN93 on these implicate its action on CaMKII [45] or CaM on phosphorylation of particular (Ser516, Ser571 and Thr594) DI-DII intracellular linker residues, or on CaM-III-IV linker interaction [35]. Phosphorylation at a protein kinase C-specific site reduced peak I_{Na} and shifted steady state inactivation $V_{1/2}$ (by −15 mV) [46]. Finally, $Na_v1.5$ N-terminal domain CaM-binding site mutations have been attributed to a downregulation of I_{Na} [47].

4. Na^+ channel inhibition by RyR-mediated Ca^{2+} release

Following RyR-mediated SR Ca^{2+} release induced by AP initiation in native skeletal muscle fibres and cardiomyocytes, bulk cytosolic $[Ca^{2+}]_i$ increases from approximately 100 nM to 1–10 µM [13–15]. The latter concentrations affected Na^+ channel function in studies using *in vitro* expression systems [48]. Here, N-(2-hydroxyethyl)ethylenediamine-N,N′,N′-triacetic acid mediated Ca^{2+} buffering (K_d = 4 µM) permitting $[Ca^{2+}]_i$ approximately 10 µM to be reached; Nitr-photo-Ca^{2+} uncaging and activating co-expressed Cav1.2 gave concordant results. All reduced maximum I_{Na} in HEK293 cells expressing $Na_v1.4$, or $Na_v1.5$ chimeras with the $Na_v1.4$ CTD, but not those expressing $Na_v1.5$ or $Na_v1.4$ chimeras with the $Na_v1.5$ CTD [42,48]. However, freshly isolated rabbit [49] and cultured rat ventricular myocytes [50] showed reduced I_{Na} with $[Ca^{2+}]_i$ elevation produced by patch electrode Ca^{2+}-BAPTA or caffeine challenge and 24 h sustained culture medium $[Ca^{2+}]$ elevations, respectively. Inactivation $V_{1/2}$s was unaffected through all these studies [48]. These differences underline the importance of conducting experimental analyses in intact native systems.

Furthermore, the modelling studies above suggested that *in vivo* $[Ca^{2+}]_{TSR}$ could reach still higher levels, sufficient for regulatory Ca^{2+}-CaM binding. Intact functioning native skeletal muscle fibres and cardiomyocytes both also demonstrated corresponding I_{Na} alterations during loose-patch clamp recording under conditions of perturbed Ca^{2+} homeostasis [51]. The latter technique avoided membrane disruptions and perturbations of $[Ca^{2+}]_i$ homeostasis arising from the measurement procedures themselves. Altered $[Ca^{2+}]_i$ homeostasis could accompany and affect results from other experimental studies, including conventional patch clamp, which further often employ Ca^{2+}-chelating EGTA- and F^--containing pipette solutions. Furthermore, loose-patch clamping additionally permits sequential and multiple recordings to be made with the same standardized pipette before and after pharmacological challenge, and studies to be made in intact *in situ* skeletal muscle fibres and cardiomyocytes, as opposed to isolated or cultured cells. Features of their reported Na^+ current, $I_{Na,}$ concurred with those obtained on earlier occasions and with results from other voltage clamp methods applied to mammalian skeletal muscle fibres [51,52]. Voltage steps from resting to sequentially depolarized test potentials provided families of I_{Na} activation records. Superimposed further pulses to a fixed depolarized level could determine the voltage dependences of the consequent channel inactivation. Records were compared before and following the perturbations of *in vivo* Ca^{2+} homeostasis.

Experiments manipulating RyR-mediated intracellular SR store Ca^{2+} release demonstrated potentially physiologically significant negative feedback regulations of $Na_v1.4$ and $Na_v1.5$ in both skeletal muscle fibres and cardiomyocytes. These employed challenge by the two RyR-mediated SR Ca^{2+} release agonists 8-CPT [53,54] and caffeine [55] and the SR Ca^{2+}-ATPase inhibitor CPA [56]. In addition, the RyR antagonist dantrolene [57] was used both by itself and in combination with those remaining agents in control studies. The latter use of agents with antagonistic actions focused their actions on their effects specifically upon local cytosolic $[Ca^{2+}]$. Exchange protein directly activated by cAMP (Epac) causes a downstream RyR phosphorylation stimulating SR Ca^{2+} release (figure 3*a*). In murine skeletal muscle fibres, the Epac activator 8-CPT (1 µM) [53,54] reduced maximum inward I_{Na} by 30–50% (figure 3*b*i,ii). RyR block by dantrolene (10 µM) abrogated these 8-CPT actions leaving I_{Na} unchanged (figure 3*c*i,ii) [58]. Both activation and inactivation half-maximal voltages $V_{1/2}$ remained unchanged through such manoeuvres (figure 3*b*iii, iv;*c*iii,iv).

8-CPT challenge similarly reduced peak I_{Na} in murine cardiac atrial and ventricular myocyte preparations (figure 3*d*i,ii) [59]. By contrast, peak I_{Na} became indistinguishable from control levels with further addition of dantrolene (10 µM; figure 3*d*iii), or in the presence of dantrolene whether alone (figure 3*d*iv) or combined with 8-CPT (figure 3*d*v). Activation and inactivation $V_{1/2}$ and k and time constants for I_{Na} recovery from inactivation remained constant through these manoeuvres [59]. 8-CPT-treated murine atrial myocytes correspondingly demonstrated spontaneous cytosolic Ca^{2+} ($[Ca^{2+}]_i$) transients, increased amplitudes of $[Ca^{2+}]_i$ transients evoked by AP excitation, and spectrofluometrically measurable spontaneous Ca^{2+} waves suggesting Ca^{2+} homeostatic changes (figure 3*e*) [54]. Finally, the same isolated hearts provided intact Langendorff-perfused preparations to assess the physiological consequences of these procedures. These studies demonstrated reduced maximum rates of atrial and ventricular AP upstroke, $(dV/dt)_{max}$, increased AP latencies and ventricular arrhythmic phenotypes on rapid pacing or extrasystolic stimuli with intracellular sharp microelectrode membrane potential recordings [59,60].

5. Reciprocal $Na_v1.4$ alterations following Ca^{2+} store release and depletion

Independent pharmacological manipulations of intracellular skeletal muscle fibre Ca^{2+} homeostasis, potentially altering $[Ca^{2+}]_{TSR}$ (figure 4*a*), yielded concordant results [62]. The RyR agonist caffeine, applied at 0.5 and 2 mM, respectively, produces a sustained activation, and a transient activation followed by inactivation, of RyR-mediated SR Ca^{2+} release, correspondingly altering $[Ca^{2+}]_i$ in mammalian skeletal muscle fibres (figure 4*b*) [61]. Electrophysiological studies showed parallel, similarly time-dependent, decreases (figure 4*d*b) and increases in I_{Na} when 0.5 and 2 mM caffeine was added before but not following establishing the loose-patch clamp seal (figure 4*c*). Dantrolene (10 µM) abrogated these effects (figure 4*e*). Applied by itself it induced small I_{Na} increases

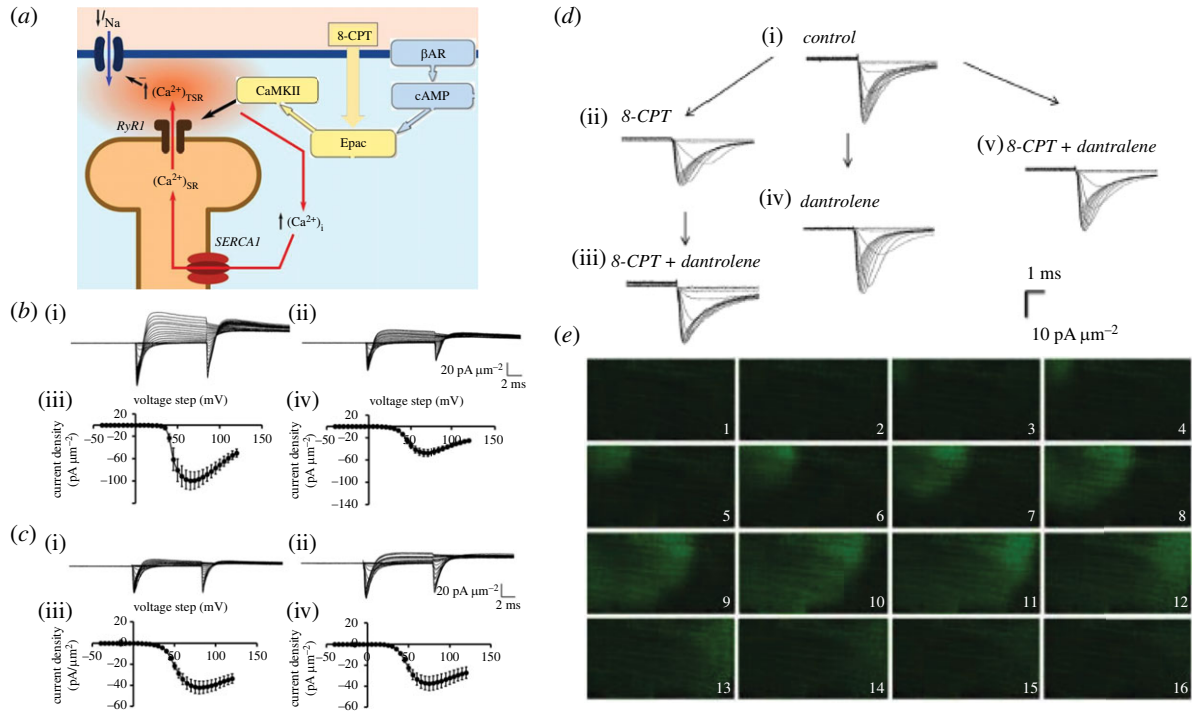

Figure 3. 8-(4-chlorophenylthio)adenosine-3′,5′-cyclic monophosphate (8-CPT) effects on Na^+ channel activation. (*a*) Scheme summarizing RyR activation through 8-CPT agonist action on Epac-mediated cAMP signalling. (*b–d*) Experimental loose-patch clamping results. (*b,c*) Ion currents in response to activating voltage steps in native murine skeletal muscle showing current families (i) before and (ii) following 8-CPT challenge. Results compared (*b*) before and (*c*) following introduction of dantrolene. (iii,iv) Corresponding current–voltage relationships. (*d*) Ion currents in experimental-isolated murine ventricular preparations (i) in the absence and (ii) presence of 8-CPT challenge before and (iii) following further addition of dantrolene, and (iv) in the presence of dantrolene alone and (v) combined with 8-CPT. (*e*) Isolated ventricular myocyte; fluo-3 images under confocal microscopy: Epac-induced wave of elevated cytosolic [Ca^{2+}]. Successive 41.0 × 20.5 µm frames each separated by 65 ms. ((*b*) From figure 3a–d, (*c*) from figure 5a–d of Matthews *et al.* [58]; (*d*) from figure 2 of Valli *et al.* [59]; (*e*) from Figure 8 of Hothi *et al.* [54] by permission.)

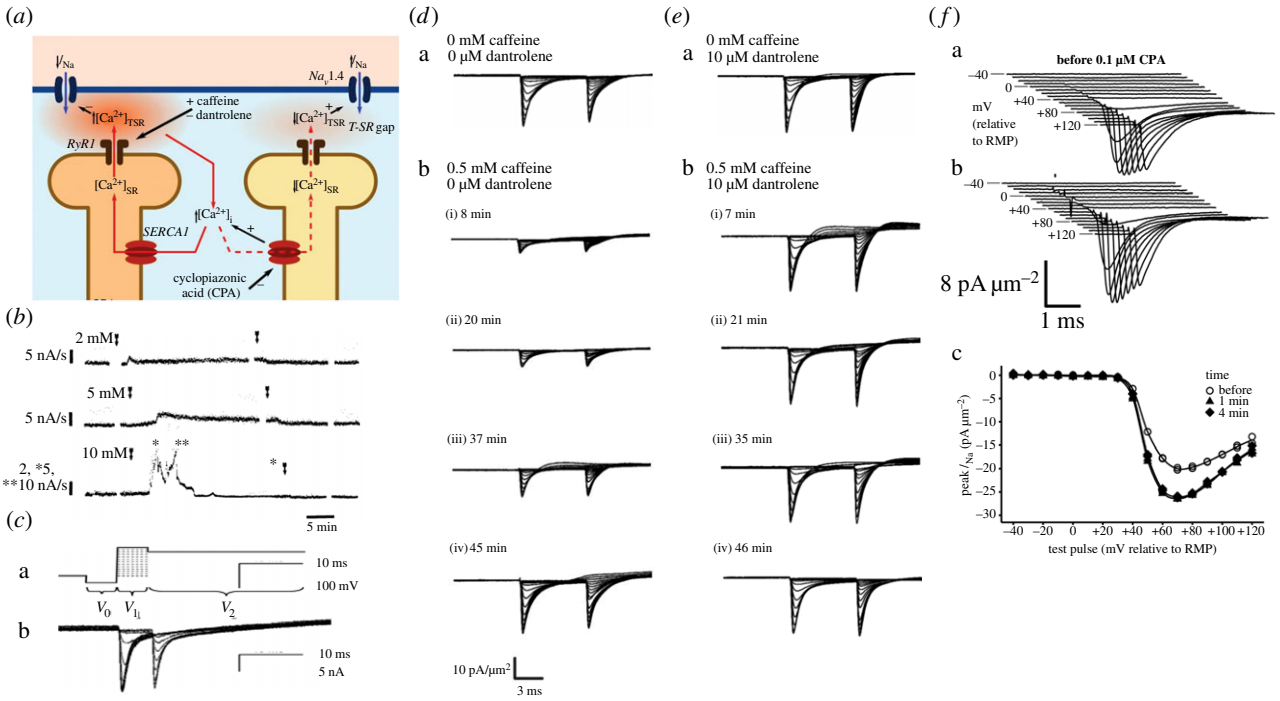

Figure 4. Paradoxical, reciprocal Na^+ current increases and decreases following caffeine and CPA-induced Ca^{2+} store release and depletion in skeletal muscle. (*a*) Possible action of caffeine induced RyR-mediated release followed by the depletion of intracellularly stored Ca^{2+} (left), and CPA-mediated store Ca^{2+} depletion by SERCA inhibition (right). This explains (*b*) varying actions of 2–10 mM caffeine on rat fast twitch muscle background aequorin Ca^{2+} signals at 25°C (arrows delimit periods of caffeine exposure) and corresponding effects of (*c*) the actions of (a) the double pulse protocols imposing families of varying depolarizing activating steps each succeeded by a step to a constant 95 mV depolarization on (b) the resulting families of loose-patch clamped murine skeletal muscle membrane currents. (*d,e*) These are illustrated (a) before and (b) at successive intervals ((i)–(iv)) after adding caffeine (0.5 mM), (*d*) before and (*e*) following addition of dantrolene (10 µM) (current densities in pA $µm^{-2}$). (*f*) Membrane currents (a) before and (b) 1 min following introduction of CPA (0.1 µM) with (c) consequent changes in I–V relationships ((*b*) from figure 2 of Fryer & Neering [61]; (*c*) from figure 1 of Valli *et al.* [59]; (*d,e*) from figure 3 of Satbjit-Singh *et al.* [62]; (*f*) from figure 3a,b,d of Liu *et al.* [63] by permission).

suggesting that it relieved inhibitory effects of a persistent resting Ca^{2+} release (figure 4*d*a,*e*a) [62].

The SR Ca^{2+}-ATPase inhibitor CPA (0.1 and 1 µM) has been similarly reported to increase bulk cytosolic $[Ca^{2+}]_i$ through a contrasting mechanism inhibiting SR Ca^{2+} re-uptake (figure 4*a*). However, I_{Na} now *increased* by approximately 30% (figure 4*f*a,b), with insignificant effects on $V_{1/2}$ and k (figure 4*f*c), within 1–4 min of introducing CPA-containing but not control solution through a bespoke flow system in identical stable membrane patches in skeletal muscle fibres [63]. CPA pre-treatment also abrogated the previously reported reductions in I_{Na} produced by 0.5 mM caffeine. In complementing results of directly modifying SR Ca^{2+} release, these paradoxical findings are compatible with reduced RyR-mediated background fluxes of SR Ca^{2+} into a T-SR $[Ca^{2+}]_i$ microdomain. This could result from SR Ca^{2+} depletion and would transiently reduce local $[Ca^{2+}]_{TSR}$. These findings thus together implicate possible local T-SR domains in which $[Ca^{2+}]_{TSR}$ was either increased or reduced in such $Na_v1.4$ down- or upregulation [63]. Finally, prolonged increases in extracellular $[Ca^{2+}]$, caffeine and CPA, expected to elevate $[Ca^{2+}]_i$, also reduced mean peak inward I_{Na} in murine atrial preparations [64].

6. Potential feedback roles in normal and abnormal skeletal muscle excitation–contraction coupling *in vivo*

The time course of the possible feedback action on $Na_v1.4$/$Na_v1.5$ by released Ca^{2+} is likely to significantly lag the electrical events within single individual AP activation and recovery cycles. Thus, within a single AP, the skeletal or cardiac muscle $Na_v1.4$- or $Na_v1.5$-mediated surface membrane excitation precedes activation of surface Ca^{2+} channel-mediated extracellular Ca^{2+} entry and/or RyR-mediated SR Ca^{2+} release. Such a timing would also extend to the significantly earlier AP recovery in skeletal muscle. The $Na_v1.4$ or $Na_v1.5$ likely subsequently undergoes inactivation before, or early within, the time course of the immediately ensuing Ca^{2+} transient, apart from possible prolonged late I_{NaL} current previously associated with $Na_v1.5$ [65]. Finally, following recovery of the cytosolic Ca^{2+} transient, much of this bound Ca^{2+} would dissociate from either the CaM or the Na_v itself, before the following AP upstroke.

Nevertheless such Ca^{2+}-mediated feedback could influence membrane excitability through the more prolonged time course of sustained, repetitive, AP activity. Thus, during cycles of repetitive AP firing, longer term, background, $[Ca^{2+}]_i$ could, respectively, increase or decrease at sustained high- or low-firing rates. This could modify $Na_v1.4$/$Na_v1.5$ function either directly or through Ca^{2+}-CaM diminishing or enhancing $Na_v1.4$/$Na_v1.5$ availability for driving AP upstroke and propagation resulting in a form of Ca^{2+} memory. $[Ca^{2+}]_i$ could also increase with compromised SR Ca^{2+}-ATPase activity following ATP depletion. In skeletal muscle, this could result in physiologically adaptive reductions in cell excitability permitting recovery from fatiguing stimulation [66]. Such effects of $[Ca^{2+}]_i$ could be physiologically important particularly under conditions of intense and prolonged muscle activation including tetanic stimulation and metabolic exhaustion. For example, tetanic stimulation in amphibian muscle was followed by significantly prolonged decays in $[Ca^{2+}]_i$ during recovery, extending even beyond full muscle relaxation. These processes could elevate $[Ca^{2+}]_i$ to even approximately 1 µM levels. Both these features were accentuated by increasing stimulation duration [67].

The presence of a Ca^{2+}-mediated feedback would predict consequences for $Na_v1.4$/$Na_v1.5$ function with clinical mutations involving the relevant functional components of either the Na^+ channel or the RyR1/RyR2. Sustained alterations in such properties appear in electrophysiological disease phenotypes associated with $Na_v1.4$ and $Na_v1.5$, CTD and III-IV linker mutations [68]. In skeletal muscle, a number of genetic $Na_v1.4$ mutations accompanying K^+ and cold-aggravated myotonias are associated with reduced Ca^{2+}-dependent Na^+ channel inhibition [48]. One such, K^+-aggravated, myotonia accompanied $Na_v1.4$ mutations in its EF-hand-like domain and was associated with slowed I_{Na} kinetics and impaired I_{Na} inactivation [69]. A further $Na_v1.4$ CTD variant clinically associated with human cold-aggravated myotonia manifesting as a transient loss of fibre excitability, myotonic stiffness and a periodic paralysis contains two amino acid substitutions, DI S5-S6 loop T323M and CTD F1705I. Whole-cell patch clamp I_{Na} in HEK293 cells expressing $Na_v1.4$-T323M were indistinguishable from wild-type (WT), consistent with a benign polymorphism. However, $Na_v1.4$-F1705I was associated with normal I_{Na} activation but slowed fast inactivation with a +8.6 mV shifted $V_{1/2}$ [70]. Similarly, one report on cultured human malignant hyperthermic skeletal myocytes with particular gain-of-function RyR1 mutations described increased slowly inactivating inward, tetrodotoxin-sensitive current [71]. Finally, the weakness observed in dystrophic muscle is associated with an elevated $[Ca^{2+}]_i$ [55].

7. Ca^{2+}-dependent $Na_v1.5$ modulation in cardiac disease models

In cardiac muscle, reductions in AP conduction velocity (CV) consequent upon loss of $Na_v1.5$ function have been implicated in specific pathological pro-arrhythmic phenotypes. Thus, some cases of the pro-arrhythmic loss of $Na_v1.5$ function Brugada Syndrome (BrS) show mutations in site B of the DIII-DIV linker [72] (figure 2*b*ii), or in the CTD, particularly its EFL sites. These could compromise capture of the DIII-DIV linker during recovery from inactivation, and of the NLBM (figure 2*a*). Contrastingly, some gain of $Na_v1.5$ function LQTS3 cases show DIII-DIV linker, site A mutations affecting residues stabilizing DIII-DIV linker binding to the inactivation site (figure 2*b*i). Other LQTS3 cases show CTD, helix 6 mutations particularly affecting the IQ motif anchoring apo-CaM (figure 2*c*iii,iv) [72]. The latter are rescued by an overexpressed CaM [73]. Both could compromise channel inactivation [72]. The one site A (Y1496) BrS-related mutation points away from the inactivation site and strongly contacts the Ca^{2+}-CaM C lobe [34].

Cardiac *RyR2*, calsequestrin (*CASQ2*), triadin (*TRDN*) or calmodulin (*CALM1*, *CALM2* and *CALM3*) mutations [74] are associated with CPVT. This predisposes to potentially fatal mono-, polymorphic or bidirectional ventricular tachycardic episodes following adrenergic stress, as well as to atrial fibrillation [75]. Experimental murine hetero- and

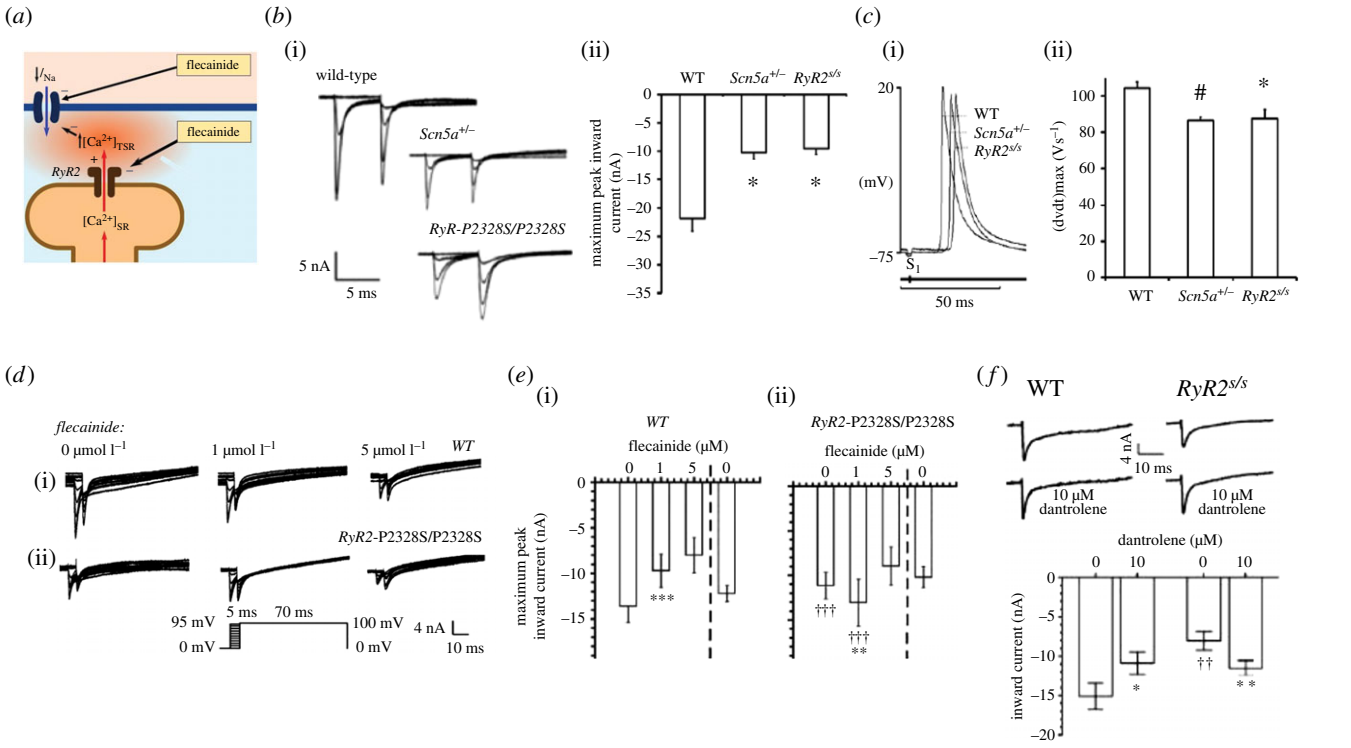

Figure 5. Na^+ current reduction in murine gain-of-function RyR2-P2328S/P2328S CPVT model and its paradoxical flecainide rescue. (*a*) Scheme for action of increased SR store Ca^{2+} release, summarizing: (*b*) loose-patch clamp membrane current results showing (i) families of WT, *Scn5a*+/— and *RyR2*-P2328S/P2328S atrial currents obtained by double pulse protocols (figure 4*ci*), and (ii) their maximum peak inward currents (*$p < 0.005$); and (*c*) the resulting (i) left atrial intracellular AP waveforms showing their conduction delays reflecting (ii) their varying maximum upstroke rates. (*d*) Membrane currents in 0, 1 and 5 µM flecainide in (i) WT and (ii) *RyR2-P2328S/P2328S* left atria. (*e*) Their respective (i,ii) maximum peak currents with exposure followed by the withdrawal of flecainide. (*f*) Parallel effects in membrane currents in response to an 80 mV depolarizing step before and following dantrolene (10 µM) challenge ((*b*) from figure 5C and (*c*) from figure 5A of King *et al.* [64]; (*d*) from figure 4(a) and (b), (*e*) from figure 3(c) and (d), (*f*) from figure 3, inset of Salvage *et al.* [76] by permission).

homozygotic *RyR2-P2328S* ventricular cardiomyocytes showed abnormal RyR2-mediated diastolic $[Ca^{2+}]_i$ elevations (figure 5*a*) [77]. Bilayer homozygotic *RyR2-P2328S* channels correspondingly exhibited enhanced channel activity at a cytoplasmic $[Ca^{2+}]$ of 1 µM as well as greater than 10-fold negative and greater than 1000-fold positive shifts in cytosolic Ca^{2+} dependences of activation and inactivation, respectively, but normal unit channel conductances [78].

Altered I_{Na} potentially could contribute to the CPVT phenotype associated with the *RyR2-P2328S* variant. Loose-patch clamp measurements in superfused homozygotic *RyR2-P2328S* atria revealed markedly reduced peak I_{Na} to extents comparable to findings in $Na_v1.5$-haploinsufficient *Scn5a*$^{+/-}$ atria (figure 5*bi*,ii). Activation and inactivation current–voltage relationships were unchanged [64]. Floating intracellular microelectrode measurements correspondingly demonstrated reduced interatrial CVs and $(dV/dt)_{max}$, but normal recovery, AP duration (APD) and refractory period values (figure 5*ci*,ii). Multi-electrode array recordings confirmed reduced atrial epicardial AP CVs [79]. Both spontaneously beating and regularly (S1) paced *RyR2-P2328S* but not WT atria correspondingly showed sustained tachyarrhythmias, delayed afterdepolarizations and ectopic APs. These likely resulted from the compromised CVs. Thus, extrasystolic, S2, stimulation provoked arrhythmia at longer S1S2 intervals in the *RyR2-P2328S* that nevertheless corresponded to similar $(dV/dt)_{max}$, and effective interatrial CVs as those provoking arrhythmia in WT [79]. Spontaneously beating *RyR2-P2328S* hearts also recapitulated clinical pro-arrhythmic ventricular phenotypes on isoproterenol and caffeine challenge [80]. These correlated with reduced ventricular $(dV/dt)_{max}$ and epicardial CVs, particularly in homo- as opposed to heterozygotic *RyR2-P2328S* and WT hearts [80].

8. A translational basis for flecainide-based catecholaminergic polymorphic ventricular tachycardic monotherapy

Rescue of the conduction slowing resulting from a Ca^{2+}-mediated reduction in I_{Na} may offer a basis for recent introduction of low-dose flecainide in CPVT therapy [81–85]. The Class Ic $Na_v1.5$ blocker flecainide (IC_{50} approx. 2–7 µM) causes a pro-arrhythmic slowing of AP conduction under conditions of $Na_v1.5$ haploinsufficiency including the BrS (review: [86]). However, more recent reports suggesting its partial reclassification as a cardiotropic drug [87–89] were prompted by its additional RyR2 inhibitory actions (IC_{50} approximately 5–11 µM) [85,90,91]. Flecainide (1 µM) exerted respective pro- and paradoxically anti-arrhythmic actions in WT and homozygotic *RyR2-P2328S* atrial preparations. In WT, flecainide (1 µM) reduced loose-patch clamp I_{Na} and slowed multi-electrode array recordings of CV while sparing refractory periods (figure 5*di*,*ei*). In *RyR2-P2328S*, it contrastingly restored I_{Na} to WT values, similarly sparing refractory periods (figure 5*d*ii,*e*ii). These effects were replicated by dantrolene challenge (10 µM; figure 5*f*). Higher flecainide concentrations (5 µM) reduced I_{Na} in both WT and *RyR2-P2328S* [76]. These findings suggest that the low-dose flecainide rescued *RyR2-P2328S* arrhythmic

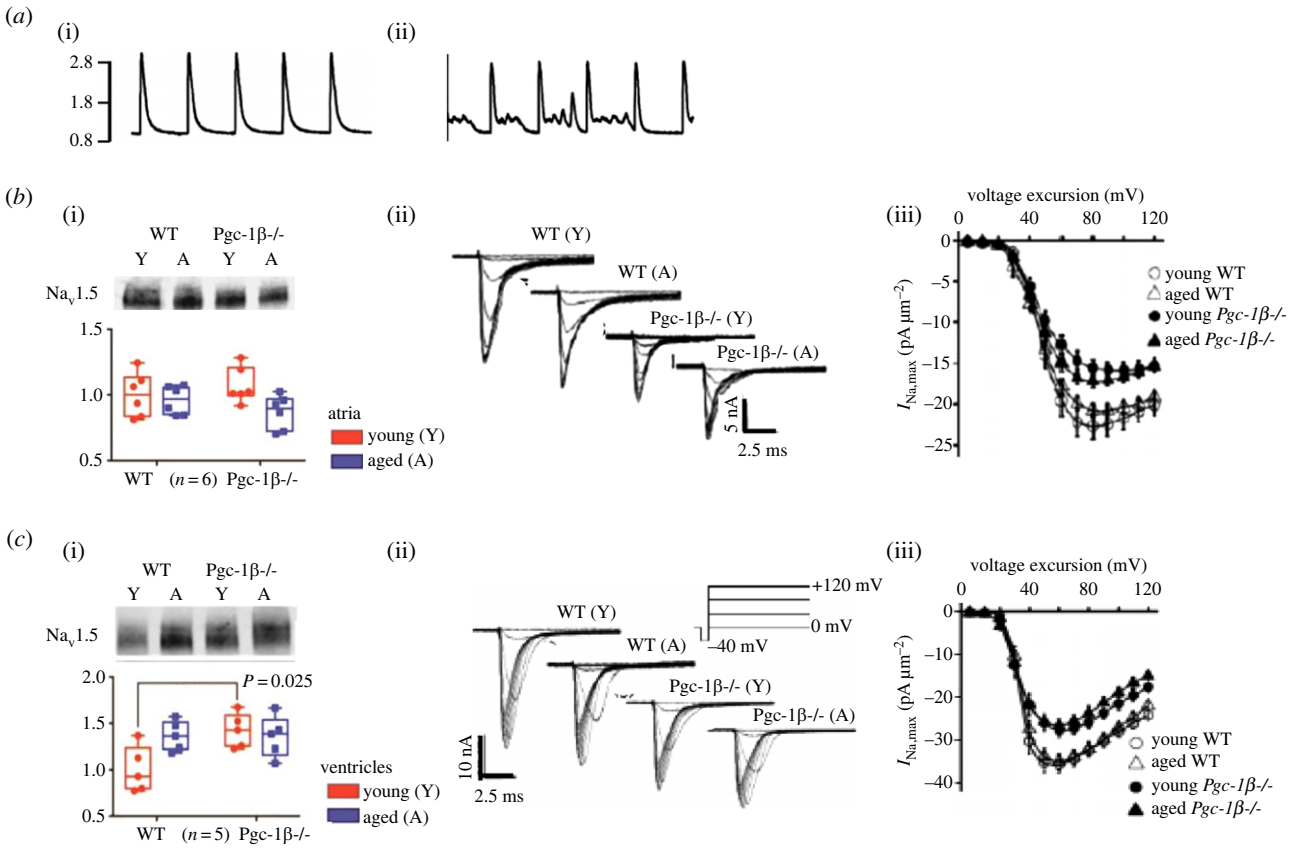

Figure 6. Altered Ca^{2+} homeostasis and I_{Na} in peroxisome proliferator-activated receptor-γ coactivator-1 (PGC-1) transcriptional coactivator deficient (Pgc-1$\beta^{-/-}$) murine cardiomyocytes. (*a*) Line scans averaged from fluorescence confocal microscopy of regularly paced (0.5 Hz), fluo-4 loaded, WT (i) and *Pgc-1β*$^{-/-}$ ventricular myocytes (ii). (*b*,*c*) Results from (i) Western blot assessments of $Na_v1.5$ expression, (ii) ion current measurements and (iii) activation current–voltage relationships in young (Y) and aged (A) WT and *Pgc-1β*$^{-/-}$ atria (*b*) and ventricles (*c*). ((*a*) from figure 3A–C of Gurung *et al.* [103]; (*b*)(i) from figure 1(A,B) and (*c*)(i) from figure 3(A,B) of Edling *et al.* [104]); (*b*)(ii) from figure 1(E–H) and (*b*)(iii) from figure 1J of Valli *et al.* [105]; (*c*)(ii) from figure 2(e–h) and (*c*)(iii) from figure 2(j) of Ahmad *et al.* [106], by permission.)

phenotypes by inhibiting RyR2-mediated Ca^{2+} elevations and their pro-arrhythmic inhibition of $Na_v1.5$. These findings may underly its translation into anti-arrhythmic clinical monotherapy for CPVT at low doses [81–85] (however, see also [88,92–95]).

9. Possible feedback effects on $Na_v1.5$ function in chronic metabolic cardiac pathology

Ageing and the age-related conditions obesity, diabetes mellitus and cardiac failure, all associated with perturbed cellular energetics, can manifest in cardiac electrophysiological changes and pro-arrhythmic phenotypes [96,97]. The peroxisome proliferator-activated receptor-γ coactivator-1 (PGC-1) transcriptional coactivators PGC-1α and PGC-1β—highly expressed in oxidative, including cardiac, tissues—are downregulated in these conditions [98]. PGC-1s regulate mitochondrial mass, function and cellular metabolism and upregulate nuclear and mitochondrial gene expression underlying fatty acid β-oxidation, the tricarboxylic acid cycle and electron transport [99]. In addition to increased reactive oxygen species production [100,101] and ATP/ADP depletion [102], recent reports implicate altered Ca^{2+} homeostasis in such pathology. Spontaneous Ca^{2+} leaks similarly occur in atrial fibrillation, cardiac failure and hypertrophic cardiomyopathies. These effects can thus be examined in genetic platforms with modified PGC-1 expression. Isolated *Pgc-1β*$^{-/-}$ murine cardiomyocytes showed altered ion channel expression and function, abnormal Ca^{2+} homeostasis and delayed after-depolarization phenomena, modelling their perturbed electrophysiological function (figure 6*a*i,ii) [103].

Pgc-1β$^{-/-}$ hearts showed reduced $Na_v1.5$ electrophysiological activity. Western blots of atrial and ventricular tissue lysates from young and old, and WT and *Pgc-1β*$^{-/-}$ mice showed similar $Na_v1.5$ expression levels except for actually greater $Na_v1.5$ expression in young *Pgc-1β*$^{-/-}$ than WT ventricles (figure 6*b*i,*c*i) [104]. Yet, loose-patch clamped myocytes in superfused *Pgc-1β*$^{-/-}$ atria and ventricles from both young and aged mice showed I_{Na} reduced compared to WT (figure 6*b*ii,*c*ii) [105,106]. The corresponding differences in current–voltage relationships related to genotype rather than age (figure 6*b*iii,*c*iii). These findings went with reduced atrial and ventricular $(dV/dt)_{max}$ and CVs, and increased arrhythmic tendency in Langendorff-perfused hearts on sharp electrode recording [107,108].

10. Feedback effects on cardiac $Na_v1.5$ function following action potential prolongation

Further extensions of hypotheses invoking Ca^{2+}-mediated feedback actions on $Na_v1.4$/$Na_v1.5$ arise from the reciprocal interactions between surface membrane ion channel activity and Ca^{2+} homeostasis [109]. In addition to variations in upstroke characteristics that result from I_{Na} actions, cardiac muscle APs can vary in their recovery durations (APDs)

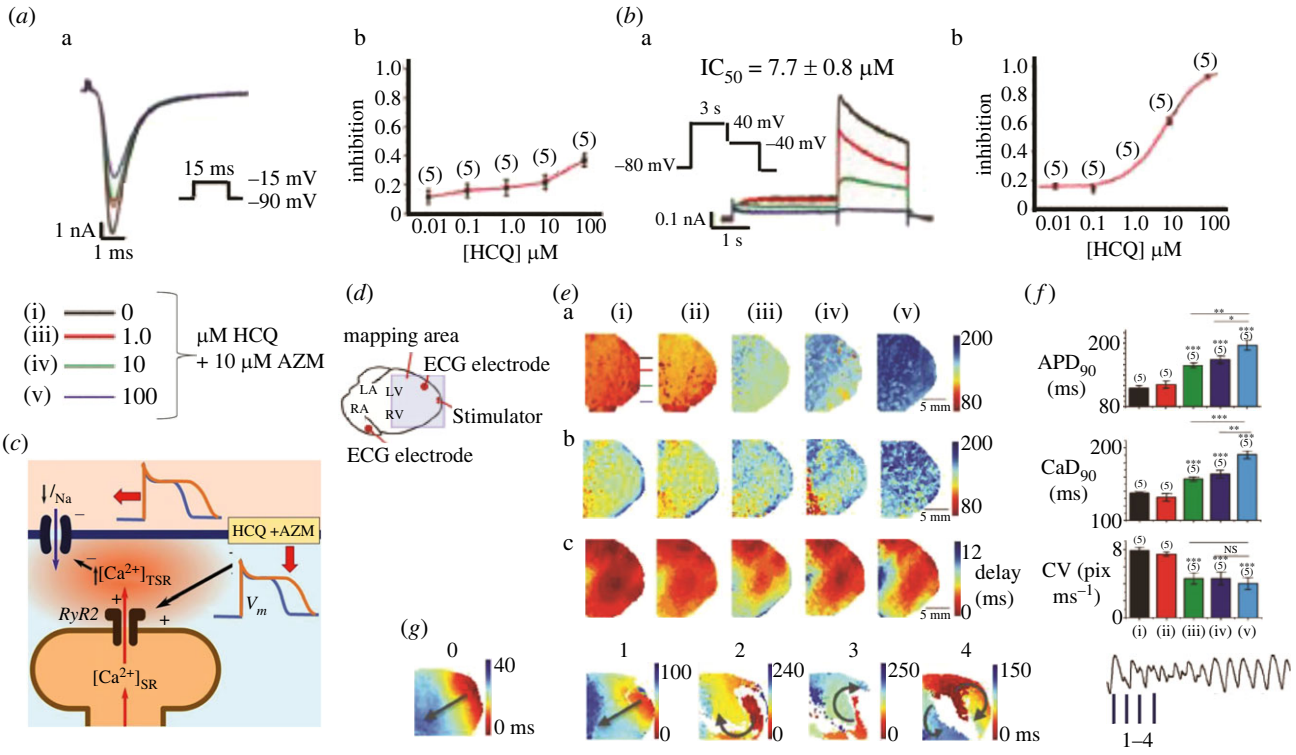

Figure 7. Effects on human (h) $Na_v1.5$ function following increases in APD secondary to HCQ and AZM challenge. (*a,b*) Effects of 0, 1, 10 and 100 μM HCQ with 10 μM AZM on $hNa_v1.5$ (I_{Na}, (*a*)) and hERG (I_{Kr}, (*b*)), showing (a) currents and (b) consequent concentration-response plots constructed from maximum magnitudes of each current in HEK293 cells. (*c*) Scheme relating these findings to (*d*) schematized mapping experiments in isolated perfused hearts with indicated optical mapping and ECG monitoring configuration. (*e*) Maps of (a) APDs at 90% repolarization (APD_{90}) measured using RH237, (b) CaD durations at 90% recovery (CaD_{90}) measured by Rhod-2 AM and (c) AP initiation and conduction measured using RH237. (*f*) The resulting (a) APD_{90}, (b) CaD_{90} and (c) CV averaged over the field of view. Comparisons in (*e,f*), made (i) before and following challenge by (ii) 1 μM and (iii) 10 μM HCQ, and 10 μM HCQ combined with either (iv) 1 or (v) 10 μM AZM. (*g*) Voltage RH237 optical mapping of re-entry and ventricular arrhythmic tendency in isolated perfused hearts paced at a 170 ms CL, before (control numbered '0') and following addition of 10 μM HCQ with added 10 μM AZM. Each map corresponds to the timepoints numbered 1–4 shown on the monitored ECG. NS not significant, $*p < 0.05$, $**p < 0.01$, $***p < 0.001$. ((*a,b*) from figure 3(A,D)(i) and (ii); (*d*) from figure 6(A)(i); (*e*)(a–c) and (*f*) from figure 6(B)(i) and (iii), (C)(i) and (iii), and (A)(i) and (iv); (*g*) from figure 7(B,C) of Wang *et al.* [109] by permission).

reflecting modifications in their I_K or I_{Ca}. One extended Ca^{2+}-mediated I_{Na} feedback hypothesis might predict that an extended AP depolarization phase associated with an increased APD could enhance RyR2-mediated Ca^{2+} release. This could result in elevated or prolonged $[Ca^{2+}]_i$ transients that in turn might exert feedback effects on $Na_v1.5$ [110].

Recent studies prompted by potential cardiac arrhythmic concerns arising from Covid-19 therapy had investigated effects of HCQ alone and combined with azithromycin (HCQ+AZM). Of these, *in vitro* electrophysiological cultured cell models [111,112] and modelling studies bearing on these drug actions on individual surface membrane ion channels [112,113] predicted potentially pro-arrhythmic behaviour. Experiments integrating biophysical studies of ion channel properties with studies of AP generation and conduction, and of Ca^{2+} homeostatic processes in intact hearts together additionally suggested Ca^{2+}-mediated feedback actions on AP generation and conduction [109].

Here, therapeutic HCQ, and particularly (HCQ+AZM), levels inhibited human-expressed I_{Kr} and I_{K1} but not I_{to} and I_{Ks}. HCQ though not (HCQ+AZM) affected I_{Na} and I_{CaL} and then only at higher IC_{50}s, in patch-clamped HEK293 cells (figure 7*a,b*). Rh237 mapping of membrane potential changes in isolated perfused guinea pig hearts (i) before and following challenge by (ii) 1 μM and (iii) 10 μM HCQ, and 10 μM HCQ combined with either (iv) 1 or (v) 10 μM AZM (figure 7*c,d*) showed that μM-HCQ expectedly increased APD_{90} (figure 7*ea,fa*) and APD (figure 7*eb,fb*). However, it also reversibly reduced left atrial and ventricular CVs. It additionally increased conduction heterogeneities on multi-electrode array mapping (figure 7*ec,fc*). ECGs were bradycardic with increased PR and QRS durations. O'Hara-Rudy modelling reproduced the APD but not the CV alterations from the *in vitro* I_{Kr}, I_{K1} and I_{Na} effects. However, Rhod-2 mapping demonstrated increased durations and dispersions of the intracellular $[Ca^{2+}]$ transients. This offers a potential mechanism for the observed downregulation of I_{Na} and CV invoking a Ca^{2+}-mediated feedback on $Na_v1.5$ function. Furthermore, (HCQ+AZM) accentuated all these effects of HCQ. It further disrupted AP propagation and induced alternans and torsades-like episodes during forced pacing (figure 7*g*) [109].

11. A broader group of Ca^{2+}-mediated feedback effects on membrane excitability?

The present findings suggest Ca^{2+}-mediated effects on $Na_v1.4$ and $Na_v1.5$ that might exert an *in vivo* feedback modulation of excitation–contraction coupling in intact native skeletal muscle fibres and cardiac myocytes. Such actions could form a subclass of a range of feedback mechanisms in which local-elevated microdomain $[Ca^{2+}]$ resulting from store Ca^{2+} release might modify surface membrane channel activity and reduce

cell excitability [114,115]. The latter in turn may constitute a subcategory of a broader group of Ca^{2+}-mediated actions including Ca^{2+}-enhanced slow RyR inactivation [116]. Thus, opening Ca^{2+}-activated K^+ channels, whether in skeletal, cardiac or smooth muscle, would hyperpolarize and similarly reduce excitability in their containing membranes. 'Big K^+' (BK) large conductance, Ca^{2+} and voltage-activated, K^+ channels have intracellular C-termini containing a gating ring comprising two RCK1 and RCK2 domains. These regulate K^+ conductance through two distinct high-affinity Ca^{2+}-binding sites in each domain [117,118]. Their opening requires both membrane depolarization and increased (µM) local $[Ca^{2+}]$ [119]. They may decrease membrane excitability in exercising skeletal muscle [66] and influence sinoatrial node firing rate and cardiac pacing *in vivo* [120,121]. Genetic modifications in their encoding *KCNMA1* lead to clinical brain and muscle dysfunction [122,123].

By contrast, small conductance (SK) K^+ channel, SK1, SK2 and SK3 [124,125], subtypes include a regulatory C-terminal CaM-binding domain. They respond to submicromolar $[Ca^{2+}]_i$ increases that could arise from RyR-induced Ca^{2+} release [126] but are not sensitive to voltage change [127,128]. Normal adult human and murine, atria and ventricles express SK2 [129]. Its exact physiological cardiac role remains uncertain. It has been suggested to contribute to repolarization in normal healthy atrial [130] though not ventricular cardiomyocytes [131]. Nevertheless it may participate in atrial pathological situations including atrial fibrillation [132]. Furthermore its expression level increases with pro-arrhythmic and hypertrophic changes [133,134] observed in both experimental and clinical ventricular failure [134,135]. Studies combining results from *in vitro* adult and neonatal cardiomyocyte preparations and intact perfused hearts demonstrated increased SK2 expression and pharmacologically detectable effects upon AP recoveries paralleling ventricular hypertrophic changes induced by angiotensin II and p21-activated kinase type 1 downregulation [136]. These proved attributable to direct effects of CaMKII and CREB-mediated signalling on the KCNN2 gene promoter. This $[Ca^{2+}]_i$-mediated SK regulation could then modify membrane potential or excitability and consequent arrhythmogenicity.

Finally, $[Ca^{2+}]$-sensitivity properties also occur in some anion channels. Thus, Ca^{2+}-activated Cl^- TMEM16A channels [137], additional to established roles in smooth muscle [138], may also function in cardiac [139] and skeletal muscle [140].

Data accessibility. This article has no additional data.

Authors' contributions. S.C.S.: conceptualization, project administration and writing—review and editing; A.F.D.: conceptualization, visualization and writing—review and editing; K.J.: project administration and writing—review and editing; T.J.: conceptualization, supervision and writing—review and editing; C.L.-H.H.: conceptualization, data curation, project administration, supervision, writing—original draft and writing—review and editing.

All authors gave final approval for publication and agreed to be held accountable for the work performed therein.

Conflict of interest declaration. We declare we have no competing interests.

Funding. We thank the British Heart Foundation (PG/14/79/31102, PG/19/59/34582) and Cambridge Centre for Research Excellence (S.C.S., A.P.J. and C.L.H.H.), Medical Research Council (MR/M001288/1, C.L.H.H.) and Wellcome Trust (105727/Z/14/Z, C.L.H.H.), and the Australian National Health and Medical Research Council (APP108477, A.F.D.), for generous support.

References

1. Huang CLH, Pedersen TH, Fraser JA. 2011 Reciprocal dihydropyridine and ryanodine receptor interactions in skeletal muscle activation. *J. Muscle Res. Cell Motil.* **32**, 171–202. (doi:10.1007/s10974-011-9262-9)
2. Endo M. 2009 Calcium-induced calcium release in skeletal muscle. *Physiol. Rev.* **89**, 1153–1176. (doi:10.1152/physrev.00040.2008)
3. Franzini-Armstrong C, Nunzi G. 1983 Junctional feet and particles in the triads of a fast-twitch muscle fibre. *J. Muscle Res. Cell Motil.* **4**, 233–252. (doi:10.1007/BF00712033)
4. Franzini-Armstrong C, Protasi F, Ramesh V. 1999 Shape, size, and distribution of Ca^{2+} release units and couplons in skeletal and cardiac muscles. *Biophys. J.* **77**, 1528–1539. (doi:10.1016/S0006-3495(99)77000-1)
5. Dulhunty AF. 2006 Excitation-contraction coupling from the 1950s into the new millennium. *Clin. Exp. Pharmacol. Physiol.* **33**, 763–772. (doi:10.1111/j.1440-1681.2006.04441.x)
6. Martin CA, Petousi N, Chawla S, Hockaday AR, Burgess AJ, Fraser JA, Huang CLH, Skepper JN. 2003 The effect of extracellular tonicity on the anatomy of triad complexes in amphibian skeletal muscle. *J. Muscle Res. Cell Motil.* **24**, 407–415. (doi:10.1023/A:1027356410698)
7. Bardsley OJ, Matthews HR, Huang CLH. 2021 Finite element analysis predicts Ca^{2+} microdomains within tubular-sarcoplasmic reticular junctions of amphibian skeletal muscle. *Sci. Rep.* **11**, 14376. (doi:10.1038/s41598-021-93083-1)
8. Despa S, Shui B, Bossuyt J, Lang D, Kotlikoff MI, Bers DM. 2014 Junctional cleft $[Ca^{2+}]$i measurements using novel cleft-targeted Ca^{2+} sensors. *Circ. Res.* **115**, 339–347. (doi:10.1161/CIRCRESAHA.115.303582)
9. Saucerman JJ, Bers DM. 2012 Calmodulin binding proteins provide domains of local Ca^{2+} signaling in cardiac myocytes. *J. Mol. Cell. Cardiol.* **52**, 312–316. (doi:10.1016/j.yjmcc.2011.06.005)
10. Sanchez C, Berthier C, Tourneur Y, Monteiro L, Allard B, Csernoch L, Jacquemond V. 2021 Detection of Ca^{2+} transients near ryanodine receptors by targeting fluorescent Ca^{2+} sensors to the triad. *J. Gen. Physiol.* **153**, e202012592. (doi:10.1085/JGP.202012592)
11. Kovacs L, Rios E, Schneider MF. 1983 Measurement and modification of free calcium transients in frog skeletal muscle fibres by a metallochromic indicator dye. *J. Physiol.* **343**, 161–196. (doi:10.1113/jphysiol.1983.sp014887)
12. Melzer W, Ríos E, Schneider MF. 1986 The removal of myoplasmic free calcium following calcium release in frog skeletal muscle. *J. Physiol.* **372**, 261–292. (doi:10.1113/jphysiol.1986.sp016008)
13. Konishi M, Watanabe M. 1995 Resting cytoplasmic free Ca^{2+} concentration in frog skeletal muscle measured with fura-2 conjugated to high molecular weight dextran. *J. Gen. Physiol.* **106**, 1123–1150. (doi:10.1085/jgp.106.6.1123)
14. Harkins AB, Kurebayashi N, Baylor SM. 1993 Resting myoplasmic free calcium in frog skeletal muscle fibers estimated with fluo-3. *Biophys. J.* **65**, 865–881. (doi:10.1016/S0006-3495(93)81112-3)
15. Kurebayashi N, Harkins AB, Baylor SM. 1993 Use of fura red as an intracellular calcium indicator in frog skeletal muscle fibers. *Biophys. J.* **64**, 1934–1960. (doi:10.1016/S0006-3495(93)81564-9)
16. Lavorato M, Huang TQ, Iyer VR, Perni S, Meissner G, Franzini-Armstrong C. 2015 Dyad content is reduced in cardiac myocytes of mice with impaired calmodulin regulation of RyR2. *J. Muscle Res. Cell Motil.* **36**, 205–214. (doi:10.1007/s10974-015-9405-5)
17. Salvage SC, Habib ZF, Matthews HR, Jackson AP, Huang CLH. 2021 Ca^{2+}-dependent modulation of voltage-gated myocyte sodium channels. *Biochem. Soc. Trans.* **49**, 1941–1961. (doi:10.1042/bst20200604)
18. Yan Z *et al.* 2017 Structure of the $Na_v1.4$-β1 complex from electric eel. *Cell* **170**, 470–482.e11. (doi:10.1016/j.cell.2017.06.039)

19. Pan X *et al.* 2018 Structure of the human voltage-gated sodium channel $Na_v1.4$ in complex with $\beta1$. *Science* **362**, eaau2486. (doi:10.1126/science.aau2486)
20. Shen H, Liu D, Wu K, Lei J, Yan N. 2019 Structures of human $Na_v1.7$ channel in complex with auxiliary subunits and animal toxins. *Science* **363**, 1303–1308. (doi:10.1126/science.aaw2493)
21. Jiang D, Shi H, Tonggu L, Gamal El-Din TM, Lenaeus MJ, Zhao Y, Yoshioka C, Zheng N, Catterall WA. 2020 Structure of the cardiac sodium channel. *Cell* **180**, 122–134.e10. (doi:10.1016/j.cell.2019.11.041)
22. West JW, Patton DE, Scheuer T, Wang Y, Goldin AL, Catterall WA. 1992 A cluster of hydrophobic amino acid residues required for fast Na^+-channel inactivation. *Proc. Natl Acad. Sci. USA* **89**, 10 910–10 914. (doi:10.1073/pnas.89.22.10910)
23. Wingo TL, Shah VN, Anderson ME, Lybrand TP, Chazin WJ, Balser JR. 2004 An EF-hand in the sodium channel couples intracellular calcium to cardiac excitability. *Nat. Struct. Mol. Biol.* **11**, 219–225. (doi:10.1038/nsmb737)
24. Chagot B, Potet F, Balser JR, Chazin WJ. 2009 Solution NMR structure of the C-terminal EF-hand domain of human cardiac sodium channel $Na_v1.5$. *J. Biol. Chem.* **284**, 6436–6445. (doi:10.1074/jbc.M807747200)
25. Gardill BR, Rivera-Acevedo RE, Tung CC, Okon M, McIntosh LP, Van Petegem F. 2018 The voltage-gated sodium channel EF-hands form an interaction with the III-IV linker that is disturbed by disease-causing mutations. *Sci. Rep.* **8**, 4483. (doi:10.1038/s41598-018-22713-y)
26. Clairfeuille T *et al.* 2019 Structural basis of α-scorpion toxin action on Na_v channels. *Science* **363**, eaav8573. (doi:10.1126/science.aav8573)
27. Pitt GS, Lee SY. 2016 Current view on regulation of voltage-gated sodium channels by calcium and auxiliary proteins. *Protein Sci.* **25**, 1573–1584. (doi:10.1002/pro.2960)
28. Shah VN, Wingo TL, Weiss KL, Williams CK, Balser JR, Chazin WJ. 2006 Calcium-dependent regulation of the voltage-gated sodium channel hH1: intrinsic and extrinsic sensors use a common molecular switch. *Proc. Natl Acad. Sci. USA* **103**, 3592–3597. (doi:10.1073/pnas.0507397103)
29. Halling DB, Liebeskind BJ, Hall AW, Aldrich RW. 2016 Conserved properties of individual Ca^{2+}-binding sites in calmodulin. *Proc. Natl Acad. Sci. USA* **113**, E1216–E1225. (doi:10.1073/pnas.1600385113)
30. Wang C, Chung BC, Yan H, Wang HG, Lee SY, Pitt GS. 2014 Structural analyses of Ca^{2+}/CaM interaction with Na_V channel C-termini reveal mechanisms of calcium-dependent regulation. *Nat. Commun.* **5**, 4896. (doi:10.1038/ncomms5896)
31. Rhoads AR, Friedberg F. 1997 Sequence motifs for calmodulin recognition. *FASEB J.* **11**, 331–340. (doi:10.1096/fasebj.11.5.9141499)
32. Tan HL, Kupershmidt S, Zhang R, Stepanovic S, Roden DM, Wilde AAM, Anderson ME, Balser JR. 2002 A calcium sensor in the sodium channel modulates cardiac excitability. *Nature* **415**, 442–447. (doi:10.1038/415442a)
33. Meador WE, Means AR, Quiocho FA. 1992 Target enzyme recognition by calmodulin: 2.4 Å structure of a calmodulin-peptide complex. *Science* **257**, 1251–1255. (doi:10.1126/science.1519061)
34. Sarhan MF, Tung CCC, Van Petegem F, Ahern CA, Clapham D. 2012 Crystallographic basis for calcium regulation of sodium channels. *Proc. Natl Acad. Sci. USA* **109**, 3558–3563. (doi:10.1073/pnas.1114748109)
35. Johnson CN, Potet F, Thompson MK, Kroncke BM, Glazer AM, Voehler MW, Knollmann BC, George AL, Chazin WJ. 2018 A mechanism of calmodulin modulation of the human cardiac sodium channel. *Structure* **26**, 683–694.e3. (doi:10.1016/j.str.2018.03.005)
36. Kim J, Ghosh S, Liu H, Tateyama M, Kass RS, Pitt GS. 2004 Calmodulin mediates Ca^{2+} sensitivity of sodium channels. *J. Biol. Chem.* **279**, 45 004–45 012. (doi:10.1074/jbc.M407286200)
37. Shah VN, Chagot B, Chazin WJ. 2006 Calcium-dependent regulation of ion channels. *Calcium Bind. Proteins* **1**, 203–212.
38. Nathan S, Gabelli SB, Yoder JB, Srinivasan L, Aldrich RW, Tomaselli GF, Ben-Johny M, Amzel LM. 2021 Structural basis of cytoplasmic $Na_v1.5$ and $Na_v1.4$ regulation. *J. Gen. Physiol.* **153**, e202012722. (doi:10.1085/jgp.202012722)
39. Chagot B, Chazin WJ. 2011 Solution NMR structure of apo-calmodulin in complex with the IQ motif of human cardiac sodium channel $Na_v1.5$. *J. Mol. Biol.* **406**, 106–119. (doi:10.1016/j.jmb.2010.11.046)
40. Feldkamp MD, Yu L, Shea MA. 2011 Structural and energetic determinants of apo calmodulin binding to the IQ motif of the $Na_v1.2$ voltage-dependent sodium channel. *Structure* **19**, 733–747. (doi:10.1016/j.str.2011.02.009)
41. Gardill BR, Rivera-Acevedo RE, Tung CC, Van Petegem F. 2019 Crystal structures of Ca^{2+}–calmodulin bound to Na_v C-terminal regions suggest role for EF-hand domain in binding and inactivation. *Proc. Natl Acad. Sci. USA* **166**, 10 763–10 772. (doi:10.1073/pnas.1818618116)
42. Yoder JB, Ben-Johny M, Farinelli F, Srinivasan L, Shoemaker SR, Tomaselli GF, Gabelli SB, Amzel LM. 2019 Ca^{2+}-dependent regulation of sodium channels $Na_v1.4$ and $Na_v1.5$ is controlled by the post-IQ motif. *Nat. Commun.* **10**, 1514. (doi:10.1038/s41467-019-09570-7)
43. Isbell HM, Kilpatrick AM, Lin Z, Mahling R, Shea MA. 2018 Backbone resonance assignments of complexes of apo human calmodulin bound to IQ motif peptides of voltage-dependent sodium channels $Na_v1.1$, $Na_v1.4$ and $Na_v1.7$. *Biomol. NMR Assign.* **12**, 283–289. (doi:10.1007/s12104-018-9824-5)
44. Potet F, Chagot B, Anghelescu M, Viswanathan PC, Stepanovic SZ, Kupershmidt S, Chazin WJ, Balser JR. 2009 Functional interactions between distinct sodium channel cytoplasmic domains through the action of calmodulin. *J. Biol. Chem.* **284**, 8846–8854. (doi:10.1074/jbc.M806871200)
45. Hund TJ *et al.* 2010 A β(IV)-spectrin/CaMKII signaling complex is essential for membrane excitability in mice. *J. Clin. Invest.* **120**, 3508–3519. (doi:10.1172/JCI43621)
46. Grandi E, Herren AW. 2014 CaMKII-dependent regulation of cardiac Na^+ homeostasis. *Front. Pharmacol.* **5**, 41. (doi:10.3389/fphar.2014.00041)
47. Wang Z *et al.* 2020 Calmodulin binds to the N-terminal domain of the cardiac sodium channel $Na_v1.5$. *Channels* **14**, 268–286. (doi:10.1080/19336950.2020.1805999)
48. Ben-Johny M, Yang PS, Niu J, Yang W, Joshi-Mukherjee R, Yue DT. 2014 Conservation of Ca^{2+}/calmodulin regulation across Na and Ca^{2+} channels. *Cell* **157**, 1657–1670. (doi:10.1016/j.cell.2014.04.035)
49. Casini S, Verkerk AO, van Borren MMGJ, van Ginneken ACG, Veldkamp MW, de Bakker JMT, Tan HL. 2009 Intracellular calcium modulation of voltage-gated sodium channels in ventricular myocytes. *Cardiovasc. Res.* **81**, 72–81. (doi:10.1093/cvr/cvn274)
50. Chiamvimonvat N, Kargacin ME, Clark RB, Duff HJ. 1995 Effects of intracellular calcium on sodium current density in cultured neonatal rat cardiac myocytes. *J. Physiol.* **483**, 307–318.
51. Almers W, Stanfield PR, Stühmer W. 1983 Lateral distribution of sodium and potassium channels in frog skeletal muscle: measurements with a patch-clamp technique. *J. Physiol.* **336**, 261–284. (doi:10.1113/jphysiol.1983.sp014580)
52. Adrian RH, Marshall MW. 1977 Sodium currents in mammalian muscle. *J. Physiol.* **268**, 223–250. (doi:10.1113/jphysiol.1977.sp011855)
53. Pereira L *et al.* 2007 The cAMP binding protein Epac modulates Ca^{2+} sparks by a Ca^{2+}/calmodulin kinase signalling pathway in rat cardiac myocytes. *J. Physiol.* **583**, 685–694. (doi:10.1113/jphysiol.2007.133066)
54. Hothi SS, Gurung IS, Heathcote JC, Zhang Y, Booth SW, Skepper JN, Grace AA, Huang CLH. 2008 Epac activation, altered calcium homeostasis and ventricular arrhythmogenesis in the murine heart. *Pflugers Arch. Eur. J. Physiol.* **457**, 253–270. (doi:10.1007/s00424-008-0508-3)
55. Lamb GD, Junankar PR, Stephenson DG. 1995 Raised intracellular [Ca^{2+}] abolishes excitation-contraction coupling in skeletal muscle fibres of rat and toad. *J. Physiol.* **489**, 349–362. (doi:10.1113/jphysiol.1995.sp021056)
56. Seidler NW, Jona I, Vegh M, Martonosi A. 1989 Cyclopiazonic acid is a specific inhibitor of the Ca^{2+}-ATPase of sarcoplasmic reticulum. *J. Biol. Chem.* **264**, 17 816–17 823.
57. Krause T, Gerbershagen MU, Fiege M, Weißhorn R, Wappler F. 2004 Dantrolene—a review of its pharmacology, therapeutic use and new developments. *Anaesthesia* **59**, 364–373. (doi:10.1111/j.1365-2044.2004.03658.x)
58. Matthews HR, Tan SRX, Shoesmith JA, Ahmad S, Valli H, Jeevaratnam K, Huang CLH. 2019 Sodium current inhibition following stimulation of exchange protein directly activated by cyclic-3′,5′-adenosine

monophosphate (Epac) in murine skeletal muscle. *Sci. Rep.* **9**, 1927. (doi:10.1038/s41598-018-36386-0)

59. Valli H, Ahmad S, Sriharan S, Dean LD, Grace AA, Jeevaratnam K, Matthews HR, Huang CLH. 2018 Epac-induced ryanodine receptor type 2 activation inhibits sodium currents in atrial and ventricular murine cardiomyocytes. *Clin. Exp. Pharmacol. Physiol.* **45**, 278–292. (doi:10.1111/1440-1681.12870)
60. Li M, Hothi SS, Salvage SC, Jeevaratnam K, Grace AA, Huang CLH. 2017 Arrhythmic effects of Epac-mediated ryanodine receptor activation in Langendorff-perfused murine hearts are associated with reduced conduction velocity. *Clin. Exp. Pharmacol. Physiol.* **44**, 686–692. (doi:10.1111/1440-1681.12751)
61. Fryer MW, Neering IR. 1989 Actions of caffeine on fast- and slow-twitch muscles of the rat. *J. Physiol.* **416**, 435–454. (doi:10.1113/jphysiol.1989.sp017770)
62. Sarbjit-Singh SS, Matthews HR, Huang CLH. 2020 Ryanodine receptor modulation by caffeine challenge modifies Na^+ current properties in intact murine skeletal muscle fibres. *Sci. Rep.* **10**, 2199. (doi:10.1038/s41598-020-59196-9)
63. Liu SX, Matthews HR, Huang CLH. 2021 Sarcoplasmic reticular Ca^{2+}-ATPase inhibition paradoxically upregulates murine skeletal muscle $Na_v1.4$ function. *Sci. Rep.* **11**, 2846. (doi:10.1038/s41598-021-82493-w)
64. King J, Wickramarachchi C, Kua K, Du Y, Jeevaratnam K, Matthews HR, Grace AA, Huang CLH, Fraser JA. 2013 Loss of $Na_v1.5$ expression and function in murine atria containing the RyR2-P2328S gain-of-function mutation. *Cardiovasc. Res.* **99**, 751–759. (doi:10.1093/cvr/cvt141)
65. Kiss D *et al.* 2021 Late Na^+ current is $[Ca^{2+}]_i$-dependent in canine ventricular myocytes. *Pharmaceuticals (Basel)* **14**, 1142. (doi:10.3390/PH14111142)
66. Allen DG, Lamb GD, Westerblad H. 2008 Skeletal muscle fatigue: cellular mechanisms. *Physiol. Rev.* **88**, 287–332. (doi:10.1152/physrev.00015.2007)
67. Cannell MB. 1986 Effect of tetanus duration on the free calcium during the relaxation of frog skeletal muscle fibres. *J. Physiol.* **376**, 203–218. (doi:10.1113/jphysiol.1986.sp016149)
68. Gabelli SB, Yoder JB, Tomaselli GF, Amzel LM. 2016 Calmodulin and Ca^{2+} control of voltage gated Na^+ channels. *Channels* **10**, 45–54. (doi:10.1080/19336950.2015.1075677)
69. Kubota T, Kinoshita M, Sasaki R, Aoike F, Takahashi MP, Sakoda S, Hirose K. 2009 New mutation of the Na channel in the severe form of potassium-aggravated myotonia. *Muscle Nerve* **39**, 666–673. (doi:10.1002/mus.21155)
70. Wu F, Gordon E, Hoffman EP, Cannon SC. 2005 A C-terminal skeletal muscle sodium channel mutation associated with myotonia disrupts fast inactivation. *J. Physiol.* **565**, 371–380. (doi:10.1113/jphysiol.2005.082909)
71. Wieland SJ, Fletcher JE, Rosenberg H, Gong QH. 1989 Malignant hyperthermia: slow sodium current in cultured human muscle cells. *Am. J. Physiol. Cell Physiol.* **257**, C759–C765. (doi:10.1152/ajpcell.1989.257.4.c759)
72. Huang W, Liu M, Yan SF, Yan N. 2017 Structure-based assessment of disease-related mutations in human voltage-gated sodium channels. *Protein Cell* **8**, 401–438. (doi:10.1007/s13238-017-0372-z)
73. Yan H, Wang C, Marx SO, Pitt GS. 2017 Calmodulin limits pathogenic Na^+ channel persistent current. *J. Gen. Physiol.* **149**, 277–293. (doi:10.1085/jgp.201611721)
74. Wleklinski MJ, Kannankeril PJ, Knollmann BC. 2020 Molecular and tissue mechanisms of catecholaminergic polymorphic ventricular tachycardia. *J. Physiol.* **598**, 2817–2834. (doi:10.1113/JP276757)
75. Zhang Y, Fraser JA, Jeevaratnam K, Hao X, Hothi SS, Grace AA, Lei M, Huang CLH. 2011 Acute atrial arrhythmogenicity and altered Ca^{2+} homeostasis in murine RyR2-P2328S hearts. *Cardiovasc. Res.* **89**, 794–804. (doi:10.1093/cvr/cvq229)
76. Salvage SC, King JH, Chandrasekharan KH, Jafferji DIG, Guzadhur L, Matthews HR, Huang CLH, Fraser JA. 2015 Flecainide exerts paradoxical effects on sodium currents and atrial arrhythmia in murine RyR2-P2328S hearts. *Acta Physiol.* **214**, 361–375. (doi:10.1111/apha.12505)
77. Goddard CA, Ghais NS, Zhang Y, Williams AJ, Colledge WH, Grace AA, Huang CLH. 2008 Physiological consequences of the *P2328S* mutation in the ryanodine receptor (*RyR2*) gene in genetically modified murine hearts. *Acta Physiol.* **194**, 123–140. (doi:10.1111/j.1748-1716.2008.01865.x)
78. Salvage SC, Gallant EM, Beard NA, Ahmad S, Valli H, Fraser JA, Huang CLH, Dulhunty AF. 2019 Ion channel gating in cardiac ryanodine receptors from the arrhythmic RyR2-P2328S mouse. *J. Cell Sci.* **132**, jcs229039. (doi:10.1242/jcs.229039)
79. King J, Zhang Y, Lei M, Grace AA, Huang CLH, Fraser JA. 2013 Atrial arrhythmia, triggering events and conduction abnormalities in isolated murine RyR2-P2328S hearts. *Acta Physiol.* **207**, 308–323. (doi:10.1111/apha.12006)
80. Zhang Y *et al.* 2013 Conduction slowing contributes to spontaneous ventricular arrhythmias in intrinsically active murine RyR2-P2328S hearts. *J. Cardiovasc. Electrophysiol.* **24**, 210–218. (doi:10.1111/jce.12015)
81. Hilliard FA, Steele DS, Laver D, Yang Z, Le Marchand SJ, Chopra N, Piston DW, Huke S, Knollmann BC. 2010 Flecainide inhibits arrhythmogenic Ca^{2+} waves by open state block of ryanodine receptor Ca^{2+} release channels and reduction of Ca^{2+} spark mass. *J. Mol. Cell. Cardiol.* **48**, 293–301. (doi:10.1016/j.yjmcc.2009.10.005)
82. Hwang HS, Hasdemir C, Laver D, Mehra D, Turhan K, Faggioni M, Yin H, Knollmann BC. 2011 Inhibition of cardiac Ca^{2+} release channels (RyR2) determines efficacy of class I antiarrhythmic drugs in catecholaminergic polymorphic ventricular tachycardia. *Circ. Arrhythm. Electrophysiol.* **4**, 128–135. (doi:10.1161/CIRCEP.110.959916)
83. Van Der Werf C *et al.* 2011 Flecainide therapy reduces exercise-induced ventricular arrhythmias in patients with catecholaminergic polymorphic ventricular tachycardia. *J. Am. Coll. Cardiol.* **57**, 2244–2254. (doi:10.1016/j.jacc.2011.01.026)
84. Salvage SC, Chandrasekharan KH, Jeevaratnam K, Dulhunty AF, Thompson AJ, Jackson AP, Huang CLH. 2018 Multiple targets for flecainide action: implications for cardiac arrhythmogenesis. *Br. J. Pharmacol.* **175**, 1260–1278. (doi:10.1111/bph.13807)
85. Watanabe H *et al.* 2009 Flecainide prevents catecholaminergic polymorphic ventricular tachycardia in mice and humans. *Nat. Med.* **15**, 380–383. (doi:10.1038/nm.1942)
86. Huang CLH. 2017 Murine electrophysiological models of cardiac arrhythmogenesis. *Physiol. Rev.* **97**, 283–409. (doi:10.1152/physrev.00007.2016)
87. Lei M, Wu L, Terrar DA, Huang CLH. 2018 Modernized classification of cardiac antiarrhythmic drugs. *Circulation* **138**, 1879–1896. (doi:10.1161/CIRCULATIONAHA.118.035455)
88. Salvage SC, Gallant EM, Fraser JA, Huang CLH, Dulhunty AF. 2021 Flecainide paradoxically activates cardiac ryanodine receptor channels under low activity conditions: a potential pro-arrhythmic action. *Cells* **10**, 2101. (doi:10.3390/cells10082101)
89. Salvage S, Huang C, Fraser J, Dulhunty A. 2022 How does flecainide impact RyR2 channel function? *J. Gen. Physiol.* **154**, e202213089. (doi:10.1085/jgp.20221)
90. Galimberti ES, Knollmann BC. 2011 Efficacy and potency of class I antiarrhythmic drugs for suppression of Ca^{2+} waves in permeabilized myocytes lacking calsequestrin. *J. Mol. Cell. Cardiol.* **51**, 760–768. (doi:10.1016/j.yjmcc.2011.07.002)
91. Heath BM *et al.* 2011 Translation of flecainide- and mexiletine-induced cardiac sodium channel inhibition and ventricular conduction slowing from nonclinical models to clinical. *J. Pharmacol. Toxicol. Methods* **63**, 258–268. (doi:10.1016/j.vascn.2010.12.004)
92. Salvage S, Gallant E, Fraser J, Huang CH, Dulhunty A. 2022 Gating of RYR2 channels from the arrhythmic RYR2-P2328S mouse heart and some unexpected actions of flecainide. *J Gen. Physiol.* **154**, e2021ecc42. (doi:10.1085/jgp.202213089)
93. Liu N *et al.* 2011 Short communication: flecainide exerts an antiarrhythmic effect in a mouse model of catecholaminergic polymorphic ventricular tachycardia by increasing the threshold for triggered activity. *Circ. Res.* **109**, 291–295. (doi:10.1161/CIRCRESAHA.111.247338)
94. Sikkel MB, Collins TP, Rowlands C, Shah M, O'Gara P, Williams AJ, Harding SE, Lyon AR, MacLeod KT. 2013 Flecainide reduces Ca^{2+} spark and wave frequency via inhibition of the sarcolemmal sodium current. *Cardiovasc. Res.* **98**, 286–296. (doi:10.1093/cvr/cvt012)

95. Bannister ML, Thomas NL, Sikkel MB, Mukherjee S, Maxwell C, MacLeod KT, George CH, Williams AJ. 2015 The mechanism of flecainide action in CPVT does not involve a direct effect on RyR2. *Circ. Res.* **116**, 1324–1335. (doi:10.1161/CIRCRESAHA.116.305347)
96. Hookana E, Junttila MJ, Puurunen VP, Tikkanen JT, Kaikkonen KS, Kortelainen ML, Myerburg RJ, Huikuri HV. 2011 Causes of nonischemic sudden cardiac death in the current era. *Heart. Rhythm.* **8**, 1570–1575. (doi:10.1016/j.hrthm.2011.06.031)
97. Yeung CY, Lam KS, Li SW, Lam KF, Tse HF, Siu CW. 2012 Sudden cardiac death after myocardial infarction in type 2 diabetic patients with no residual myocardial ischemia. *Diabetes Care* **35**, 2564–2569. (doi:10.2337/dc12-0118)
98. Dillon LM, Rebelo AP, Moraes CT. 2012 The role of PGC-1 coactivators in aging skeletal muscle and heart. *IUBMB Life* **64**, 231–241. (doi:10.1002/iub.608)
99. Arany Z *et al.* 2005 Transcriptional coactivator PGC-1 alpha controls the energy state and contractile function of cardiac muscle. *Cell Metab.* **1**, 259–271. (doi:10.1016/j.cmet.2005.03.002)
100. Brown DA, O'Rourke B. 2010 Cardiac mitochondria and arrhythmias. *Cardiovasc. Res.* **88**, 241–249.
101. Sovari AA *et al.* 2013 Mitochondria oxidative stress, connexin-43 remodeling, and sudden arrhythmic death. *Circ. Arrhythmia Electrophysiol.* **6**, 623–631. (doi:10.1161/CIRCEP.112.976787)
102. Fischbach PS, White A, Barrett TD, Lucchesi BR. 2004 Risk of ventricular proarrhythmia with selective opening of the myocardial sarcolemmal versus mitochondrial ATP-gated potassium channel. *J. Pharmacol. Exp. Ther.* **309**, 554–559. (doi:10.1124/jpet.103.060780)
103. Gurung I *et al.* 2011 Deletion of the metabolic transcriptional coactivator PGC1β induces cardiac arrhythmia. *Cardiovasc. Res.* **92**, 29–38. (doi:10.1093/cvr/cvr155)
104. Edling CE, Fazmin IT, Saadeh K, Chadda KR, Ahmad S, Valli H, Huang CLH, Jeevaratnam K. 2019 Molecular basis of arrhythmic substrate in ageing murine peroxisome proliferator-activated receptor γ co-activator deficient hearts modelling mitochondrial dysfunction. *Biosci. Rep.* **39**, BSR20190403. (doi:10.1042/BSR20190403)
105. Valli H, Ahmad S, Jiang AY, Smyth R, Jeevaratnam K, Matthews HR, Huang CLH. 2018 Cardiomyocyte ionic currents in intact young and aged murine Pgc-1$\beta^{-/-}$atrial preparations. *Mech. Ageing Dev.* **169**, 1–9. (doi:10.1016/j.mad.2017.11.016)
106. Ahmad S, Valli H, Smyth R, Jiang AY, Jeevaratnam K, Matthews HR, Huang CLH. 2019 Reduced cardiomyocyte Na^+ current in the age-dependent murine Pgc-1$\beta^{-/-}$ model of ventricular arrhythmia. *J. Cell. Physiol.* **234**, 3921–3932. (doi:10.1002/jcp.27183)
107. Ahmad S, Valli H, Chadda KR, Cranley J, Jeevaratnam K, Huang CLH. 2018 Ventricular pro-arrhythmic phenotype, arrhythmic substrate, ageing and mitochondrial dysfunction in peroxisome proliferator activated receptor-γ coactivator-1β deficient (Pgc-1β—/—) murine hearts. *Mech. Ageing Dev.* **173**, 92–103. (doi:10.1016/j.mad.2018.05.004)
108. Valli H, Ahmad S, Chadda KR, Al-Hadithi ABAK, Grace AA, Jeevaratnam K, Huang CLH. 2017 Age-dependent atrial arrhythmic phenotype secondary to mitochondrial dysfunction in Pgc-1β deficient murine hearts. *Mech. Ageing Dev.* **167**, 30–45. (doi:10.1016/j.mad.2017.09.002)
109. Wang G *et al.* 2021 Electrophysiological and proarrhythmic effects of hydroxychloroquine challenge in guinea-pig hearts. *ACS Pharmacol. Transl. Sci.* **4**, 1639–1653. (doi:10.1021/acsptsci.1c00166)
110. Lei M, Huang CLH. 2020 Cardiac arrhythmogenesis: a tale of two clocks? *Cardiovasc. Res.* **116**, e205–e209. (doi:10.1093/cvr/cvz283)
111. Thomet U, Amuzescu B, Knott T, Mann SA, Mubagwa K, Radu BM. 2021 Assessment of proarrhythmogenic risk for chloroquine and hydroxychloroquine using the CiPA concept. *Eur. J. Pharmacol.* **913**, 174632. (doi:10.1016/j.ejphar.2021.174632)
112. Okada Ji, Yoshinaga T, Washio T, Sawada K, Sugiura S, Hisada T. 2021 Chloroquine and hydroxychloroquine provoke arrhythmias at concentrations higher than those clinically used to treat COVID-19: a simulation study. *Clin. Transl. Sci.* **14**, 1092–1100. (doi:10.1111/cts.12976)
113. Michaud V, Dow P, Al Rihani SB, Deodhar M, Arwood M, Cicali B, Turgeon J. 2021 Risk assessment of drug-induced long QT syndrome for some COVID-19 repurposed drugs. *Clin. Transl. Sci.* **14**, 20–28. (doi:10.1111/cts.12882)
114. Berridge MJ. 2006 Calcium microdomains: organization and function. *Cell Calcium* **40**, 405–412. (doi:10.1016/J.CECA.2006.09.002)
115. Fakler B, Adelman JP. 2008 Control of KCa channels by calcium nano/microdomains. *Neuron* **59**, 873–881. (doi:10.1016/J.NEURON.2008.09.001)
116. Laver DR, Curtis BA. 1996 Response of ryanodine receptor channels to Ca^{2+} steps produced by rapid solution exchange. *Biophys. J.* **71**, 732–741. (doi:10.1016/S0006-3495(96)79272-X)
117. Zeng XH, Xia XM, Lingle CJ. 2005 Divalent cation sensitivity of BK channel activation supports the existence of three distinct binding sites. *J. Gen. Physiol.* **125**, 273–286. (doi:10.1085/jgp.200409239)
118. Sancho M, Kyle BD. 2021 The large-conductance, calcium-activated potassium channel: a big key regulator of cell physiology. *Front. Physiol.* **12**, 750615. (doi:10.3389/fphys.2021.750615)
119. Yang H, Zhang G, Cui J. 2015 BK channels: multiple sensors, one activation gate. *Front. Physiol.* **6**, 29. (doi:10.3389/fphys.2015.00029)
120. Meredith AL, Wu Y, Gao Z, Anderson ME, Dalziel JE, Lai MH. 2014 BK channels regulate sinoatrial node firing rate and cardiac pacing *in vivo*. *Am. J. Physiol. Hear. Circ. Physiol.* **307**, H1327–H1338. (doi:10.1152/ajpheart.00354.2014)
121. Pineda S *et al.* 2021 Conserved role of the large conductance calcium-activated potassium channel, KCa1.1, in sinus node function and arrhythmia risk. *Circ. Genomic Precis. Med.* **14**, e003144. (doi:10.1161/CIRCGEN.120.003144)
122. Bailey CS, Moldenhauer HJ, Park SM, Keros S, Meredith AL. 2019 KCNMA1-linked channelopathy. *J. Gen. Physiol.* **151**, 1173–1189. (doi:10.1085/JGP.201912457)
123. He C, Li X, Wang M, Zhang S, Liu H. 2021 Deletion of BK channels decreased skeletal and cardiac muscle function but increased smooth muscle contraction in rats. *Biochem. Biophys. Res. Commun.* **570**, 8–14. (doi:10.1016/j.bbrc.2021.07.027)
124. Weisbrod D. 2020 Small and intermediate calcium activated potassium channels in the heart: role and strategies in the treatment of cardiovascular diseases. *Front. Physiol.* **11**, 590534. (doi:10.3389/FPHYS.2020.590534)
125. Adelman JP, Maylie J, Sah P. 2012 Small-conductance Ca^{2+}-activated K^+ channels: form and function. *Annu. Rev. Physiol.* **74**, 245–269. (doi:10.1146/ANNUREV-PHYSIOL-020911-153336)
126. Neelands TR, Herson PS, Jacobson D, Adelman JP, Maylie J. 2001 Small-conductance calcium-activated potassium currents in mouse hyperexcitable denervated skeletal muscle. *J. Physiol.* **536**, 397–407. (doi:10.1111/j.1469-7793.2001.0397c.xd)
127. Schumacher MA, Rivard AF, Bächinger HP, Adelman JP. 2001 Structure of the gating domain of a Ca^{2+}-activated K^+ channel complexed with Ca^{2+}/calmodulin. *Nature* **410**, 1120–1124. (doi:10.1038/35074145)
128. Maylie J, Bond CT, Herson PS, Lee WS, Adelman JP. 2004 Small conductance Ca^{2+}-activated K^+ channels and calmodulin. *J. Physiol.* **554**, 255–261. (doi:10.1113/jphysiol.2003.049072)
129. Schmitt N, Grunnet M, Olesen S. 2014 Cardiac potassium channel subtypes: new roles in repolarization and arrhythmia. *Physiol. Rev.* **94**, 609–653. (doi:10.1152/physrev.00022.2013)
130. Skibsbye L *et al.* 2014 Small-conductance calcium-activated potassium (SK) channels contribute to action potential repolarization in human atria. *Cardiovasc. Res.* **103**, 156–167. (doi:10.1093/cvr/cvu121)
131. Nagy N *et al.* 2009 Does small-conductance calcium-activated potassium channel contribute to cardiac repolarization? *J. Mol. Cell. Cardiol.* **47**, 656–663. (doi:10.1016/j.yjmcc.2009.07.019)
132. Healey JS, Morillo CA, Connolly SJ. 2005 Role of the renin-angiotensin-aldosterone system in atrial fibrillation and cardiac remodeling. *Curr. Opin. Cardiol.* **20**, 31–37. (doi:10.1097/01.hco.0000147883.32107.1d)
133. Chang PC, Chen PS. 2015 SK channels and ventricular arrhythmias in heart failure. *Trends Cardiovasc. Med.* **25**, 508–514. (doi:10.1016/J.TCM.2015.01.010)
134. Gu M, Zhu Y, Yin X, Zhang DM. 2018 Small-conductance Ca^{2+}-activated K^+ channels: insights

into their roles in cardiovascular disease. *Exp. Mol. Med.* **50**, 1–7. (doi:10.1038/S12276-018-0043-Z)

135. Terentyev D, Rochira JA, Terentyeva R, Roder K, Koren G, Li W. 2014 Sarcoplasmic reticulum Ca^{2+} release is both necessary and sufficient for SK channel activation in ventricular myocytes. *Am. J. Physiol. Heart Circ. Physiol.* **306**, H738–H746. (doi:10.1152/AJPHEART.00621.2013)
136. Yang B *et al.* 2021 Ventricular SK2 upregulation following angiotensin II challenge: modulation by p21-activated kinase-1. *J. Mol. Cell. Cardiol.* **164**, 110–125. (doi:10.1016/J.YJMCC.2021.11.001)
137. Yang T, Colecraft HM. 2016 Calmodulin regulation of TMEM16A and 16B Ca^{2+}-activated chloride channels. *Channels (Austin)* **10**, 38–44. (doi:10.1080/19336950.2015.1058455)
138. Manoury B, Tamuleviciute A, Tammaro P. 2010 TMEM16A/anoctamin 1 protein mediates calcium-activated chloride currents in pulmonary arterial smooth muscle cells. *J. Physiol.* **588**, 2305–2314. (doi:10.1113/JPHYSIOL.2010.189506)
139. Horváth B *et al.* 2016 Sarcolemmal Ca^{2+}-entry through L-type Ca^{2+} channels controls the profile of Ca^{2+}-activated Cl^- current in canine ventricular myocytes. *J. Mol. Cell. Cardiol.* **97**, 125–139. (doi:10.1016/J.YJMCC.2016.05.006)
140. Dayal A, Ng SFJ, Grabner M. 2019 Ca^{2+}-activated Cl^- channel TMEM16A/ANO1 identified in zebrafish skeletal muscle is crucial for action potential acceleration. *Nat. Commun.* **10**, 115. (doi:10.1038/S41467-018-07918-Z)